Hindawi
Structural Control and Health Monitoring
Volume 2023, Article ID 3985363, 26 pages
https://doi.org/10.1155/2023/3985363

Research Article

A Novel Application of Magnetorheological Seat Suspension with an Improved Tuning Control Strategy

Yuxuan Liang,[1,2] Xiaomin Dong,[1] Wai Kei Ao,[2] and Yi-Qing Ni[2]

[1]*College of Mechanical and Vehicle Engineering, Chongqing University, Chongqing 400030, China*
[2]*National Rail Transit Electrification and Automation Engineering Technology Research Center, Hong Kong Polytechnic University, Hong Kong 999077, China*

Correspondence should be addressed to Xiaomin Dong; xmdong@cqu.edu.cn and Wai Kei Ao; waikei.ao@polyu.edu.hk

Received 16 June 2023; Revised 19 October 2023; Accepted 6 November 2023; Published 23 November 2023

Academic Editor: Jun Li

During the operation of commercial vehicles, drivers are usually exposed to long-term vibrations and acquire several health problems. Moreover, the end-stop impacts caused by large-magnitude vibrations or shocks may affect driving performance and result in injuries. A study of magnetorheological (MR) seat suspension controlled by a novel tuning control strategy is conducted in this research to reduce vibrations and avoid end-stop impacts. First, the MR damper's characteristics are tested, and a mathematical model of MR seat suspension is established. Then, an improved tuning control strategy is designed based on this model. The proposed strategy has three control stages that can be adjusted according to the suspension stroke to improve seat comfort or avoid end-stop impacts. Each part of the control strategy is designed separately, and the vibration attenuation performance of this seat suspension is evaluated with a simulation for three excitations, i.e., harmonic excitation, bump excitation, and random road excitation. Finally, an experiment is conducted to verify the conclusion of the simulation. The seat suspension with the proposed control shows good performances on vibration attenuation and end-stop impact reduction. Compared with a passive seat, the vibration level is reduced by around 27% and end-stop impact is avoided when semiactive suspension with the proposed strategy is used. It also shows the best overall performance among the three experimental algorithms. Both the simulation and the experiment results indicate that the vibration attenuation performance of the seat suspension can be greatly improved with the improved tuning control strategy.

1. Introduction

Drivers of commercial vehicles such as trucks or agricultural vehicles are frequently exposed to various vibrations resulting from poor working conditions. These vibrations can lead to several health issues, including lumbago and backache [1, 2]. Prolonged exposure to vibrations can also result in driver fatigue, which can negatively impact concentration and driving performance [3]. As a result, it is critical to prioritize driver protection and mitigate the adverse effects of vibrations

One effective approach to address this issue is the development of vehicle seat suspension systems. Seat suspension plays a pivotal role in enhancing driver comfort and reducing the transmission of vibrations. There are three main categories of seat suspension systems: passive seat suspension [4–6], semiactive seat suspension [7–9], and active seat suspension [10–12]. Among these, the semiactive seat suspension system proposed by Karnoop [13] has garnered significant attention due to its adaptability to different working conditions and favorable cost-effectiveness compared to active systems [14]. One promising technology in this realm is the application of magnetorheological (MR) damper [15–17], which enables fast response and a wide force range [18, 19]. Extensive research has been conducted to enhance the performance of MR seat suspension systems. Song proposed new control strategies and comforts with consideration of MR suspension [20]. The authors of [21] studied a seat suspension system based on a rotary MR damper in conjunction with fuzzy control.

In addition to the mechanical system design, considerable efforts have been devoted to the control strategy of MR seat suspension systems. Traditional approaches such as Skyhook control [13] and acceleration-driven-damper (ADD) control [22] have been employed, but they have limitations in addressing different frequency ranges of vibrations [23]. To overcome these limitations, the Sky-ADD control strategy was developed to combine the advantages of both approaches across different frequency ranges [23]. Additionally, challenges related to jerking motions caused by binary logic control have also been tackled. A continuous Skyhook control strategy was proposed to mitigate these issues [24]. Moreover, advanced techniques such as hardware-in-the-loop simulation (HILS) and nonlinear control have been explored and applied to enhance control performance [18, 25, 26]. Furthermore, modern control algorithms, including linear quadratic regulator (LQR) [27], H∞ control [24, 28], sliding mode control, and fuzzy control [29, 30], have been utilized to improve accuracy and performance. In recent years, the emergence of artificial intelligence and deep learning has led to the exploration of intelligent control strategies for seat suspension systems [31–33]. Through artificial intelligence, more accurate model and control predictions can be accomplished.

According to the above research, it is crucial for seat suspension systems to provide appropriate damping characteristics according to different working conditions while maintaining smooth damping variations to reduce jerk effects during vibrations [34]. However, when a seat suspension system with low damping encounters high-magnitude vibrations or severe shocks, the available stroke may become exhausted, leading to end-stop impacts. These impacts directly transmit shocks to the driver, causing significant discomfort or harm [3]. Therefore, it is necessary to impose high damping when the seat suspension reaches stroke saturation. The primary objectives of seat suspension control are to reduce the vertical acceleration of the seat and prevent end-stop impacts.

This paper presents a study of an MR semiactive seat suspension system controlled by an improved tuning control strategy. By changing different control stages according to the relative displacement of the seat suspension, the MR seat suspension system can reduce the vibration and avoid end-stop impacts under different working conditions. Section 2 describes how a mathematical model of prototyped seat suspension is established with the performance test of the MR damper including the dynamic analysis of the suspension. Then, the detailed logic and design of the proposed control are presented in Section 3. An experiment with a vibration test bench is also conducted to verify the MR damper with the improved tuning control, which is presented in Section 4. Finally, Section 5 gives the discussions and conclusions.

2. Mechanism and Modeling of the Seat Suspension System

2.1. Characteristics of the Seat Suspension System. Figure 1 shows the prototype seat suspension, which includes guiding mechanisms, an air spring, an MR damper, and limit buffers. The tension-compression deformation of the air spring and the damper in this seat is not linear with the change in the relative height of the suspension top plate and base plate due to the complex structure. To improve the accuracy of the algorithm, a physical model reflecting the movement characteristics of the air spring and the damper is used, as shown in Figure 1(b).

The suspension height is H_0; OA = OB = $l1$; and OC = OD = $l2$. The horizontal distance between A and the centroid at the top plate is $l5$, and the horizontal distance between the air spring installation points G and C is $l6$. OF = $l3$, OE = $l4$, the metal structures OE and OF are simplified as light rods, and their angles with OB are γ and η. The angle between BC and the horizontal direction is σ, the angle between the air spring EG and the horizontal direction is φ, and the angle between the damper and the horizontal direction is θ.

"The air spring pressure can be adjusted using a button, while the initial seat height is set in the middle stroke position. The seat suspension consists of beams 1 (BC) and 2 (AD) connected to the seat, with a hinge at point O. Fixed joints A and C are vertically aligned, and the air spring EG is connected to BC. The damper DF is also connected to BC and mounted on the slider D. Vertical excitation causes relative movement between the top and base plates, and the MR damper is compressed and stretched dissipating vibration energy. The damping of the MR damper can be adjusted by changing the current applied to it, which is controlled by a controller based on different working conditions. Therefore, the damping of the seat suspension can be controlled by adjusting the damping of the MR damper."

2.2. Characterization of MR Damper Prototype. A schematic of the MR damper is shown in Figure 2. The MR damper consists of a piston, guide frame, shaft, floating piston, and MR fluid. By applying current, the coils generate a magnetic field, allowing for adjustable damping. To accurately model a seat suspension system, a mathematical model is needed to evaluate laboratory tests on an MR damper.

To verify the damping of seat suspension, the prototype is characterized by testing, which is shown in Figure 3.

The MR damper is attached to an MTS system controlled by a computer. The MTS landmark load frame 370.1 is utilized, providing a maximum output of 100 kN and a vertical test space of 1283 mm. Force data are recorded and saved by a computer connected to the MTS system. The MR damper is excited using a harmonic signal with an amplitude of 10 mm. Current inputs of 0 A, 0.4 A, 0.8 A, 1.2 A, and 1.6 A are applied to the MR damper, while the frequency of the harmonic signal is set to 1.6 Hz, 2.4 Hz, 3.2 Hz, and 4 Hz, respectively. The results are presented in Figure 4.

Figure 4 shows the force-speed loops becoming smooth with the rising of the excitation frequency. The enclosed area of the force-displacement curve increases when the current rises. Then, the damping force with the same current is slightly different up to 10% during the varying excitation frequency. Hence, the influence of the vibration frequency on the damping force is ignored to reduce the computational difficulty.

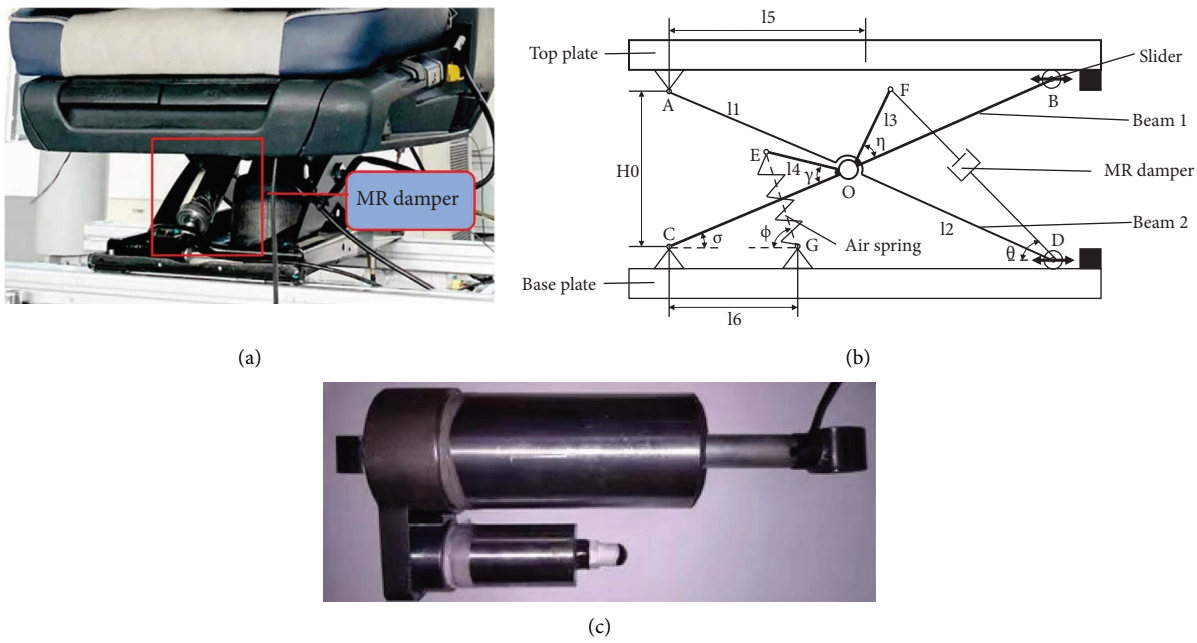

Figure 1: MR seat suspension prototype. (a) Photo of the MR damper seat suspension. (b) Conceptual diagram of seat suspension. (c) MR damper picture.

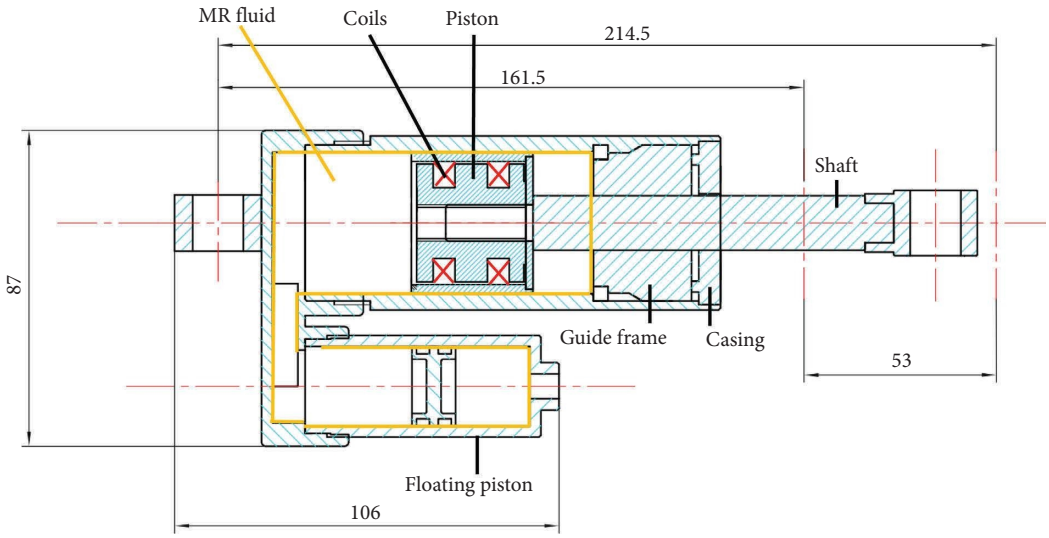

Figure 2: Schematic of the MR damper.

In this study, a hysteretic model [35] for MR fluid is used to identify characteristics of damping variability. A schematic plot is shown in Figure 5, which can be presented as follows:

$$F = c_0\dot{x} + k_0 x + \alpha \tanh\left(\beta\dot{x} + \delta \operatorname{sign}(x)\right) + f_0, \tag{1}$$

where c_0 and k_0 are the viscous and stiffness coefficients, α is the scale factor, $\tanh(\beta\dot{x} + \delta\operatorname{sign}(x))$ is the hysteretic variable, and f_0 is the damper force offset. All of the parameters are identified by MATLAB, and the results are shown in Table 1.

With the fitting tool in MATLAB, relationships between each parameter value and the current can be generated with

$$\begin{cases} c_0 = 0.0005 \cdot I + 0.0004, \\ k_0 = -0.0015 \cdot I + 0.0022, \\ \alpha = 0.2061 \cdot I^2 + 0.0919 \cdot I + 0.0908, \\ \beta = -0.0337 \cdot I + 0.0849, \\ \delta = -0.3669 \cdot I + 1.1665. \end{cases} \tag{2}$$

The damping force F can be calculated according to the hysteretic model with

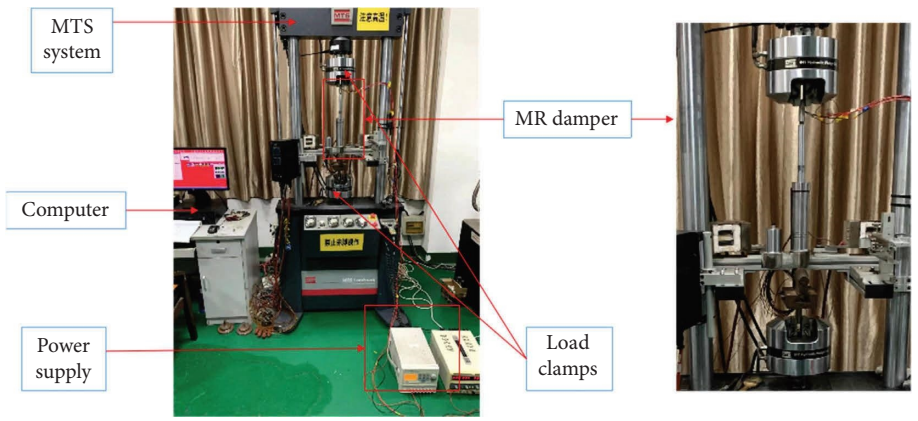

Figure 3: MR damper test system.

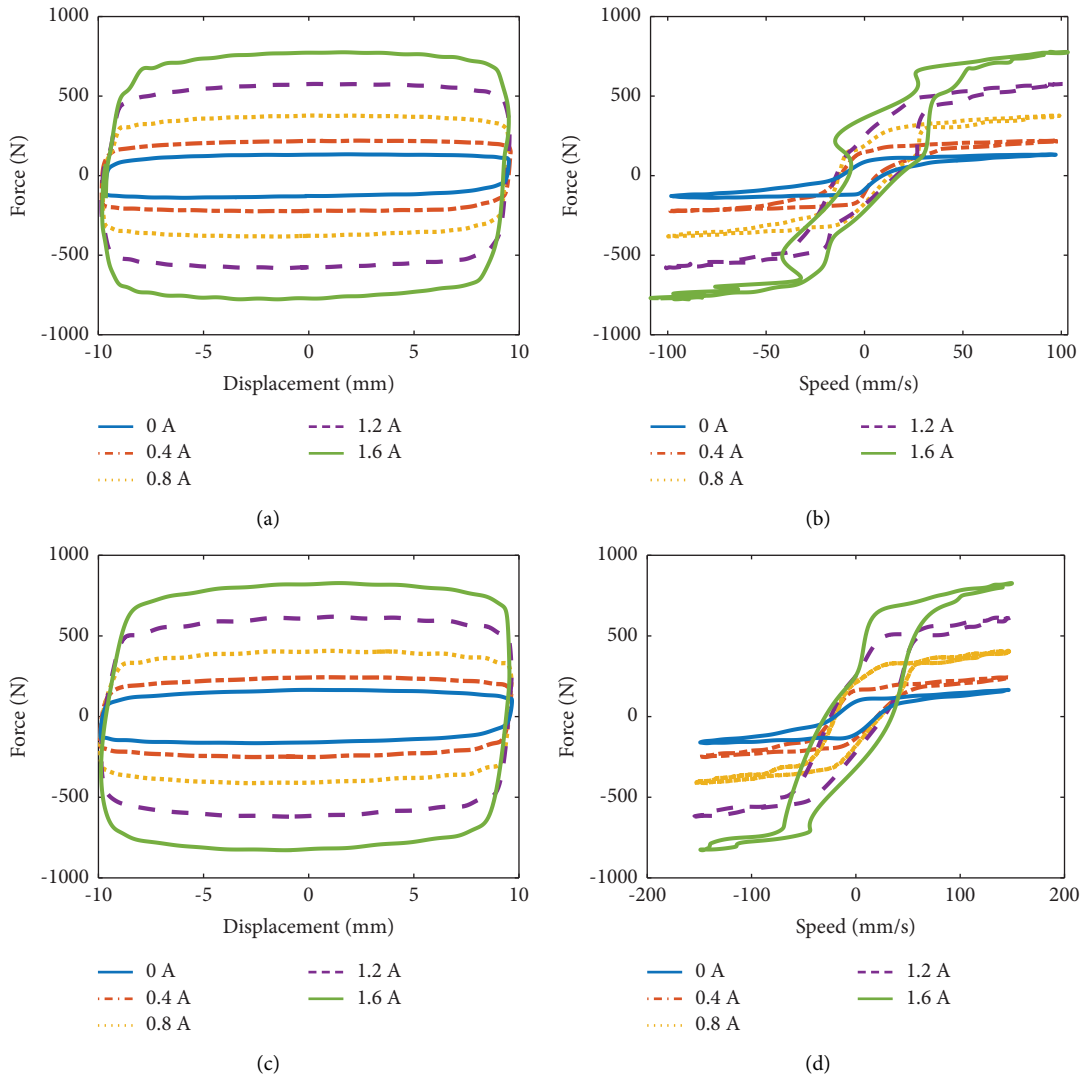

Figure 4: Continued.

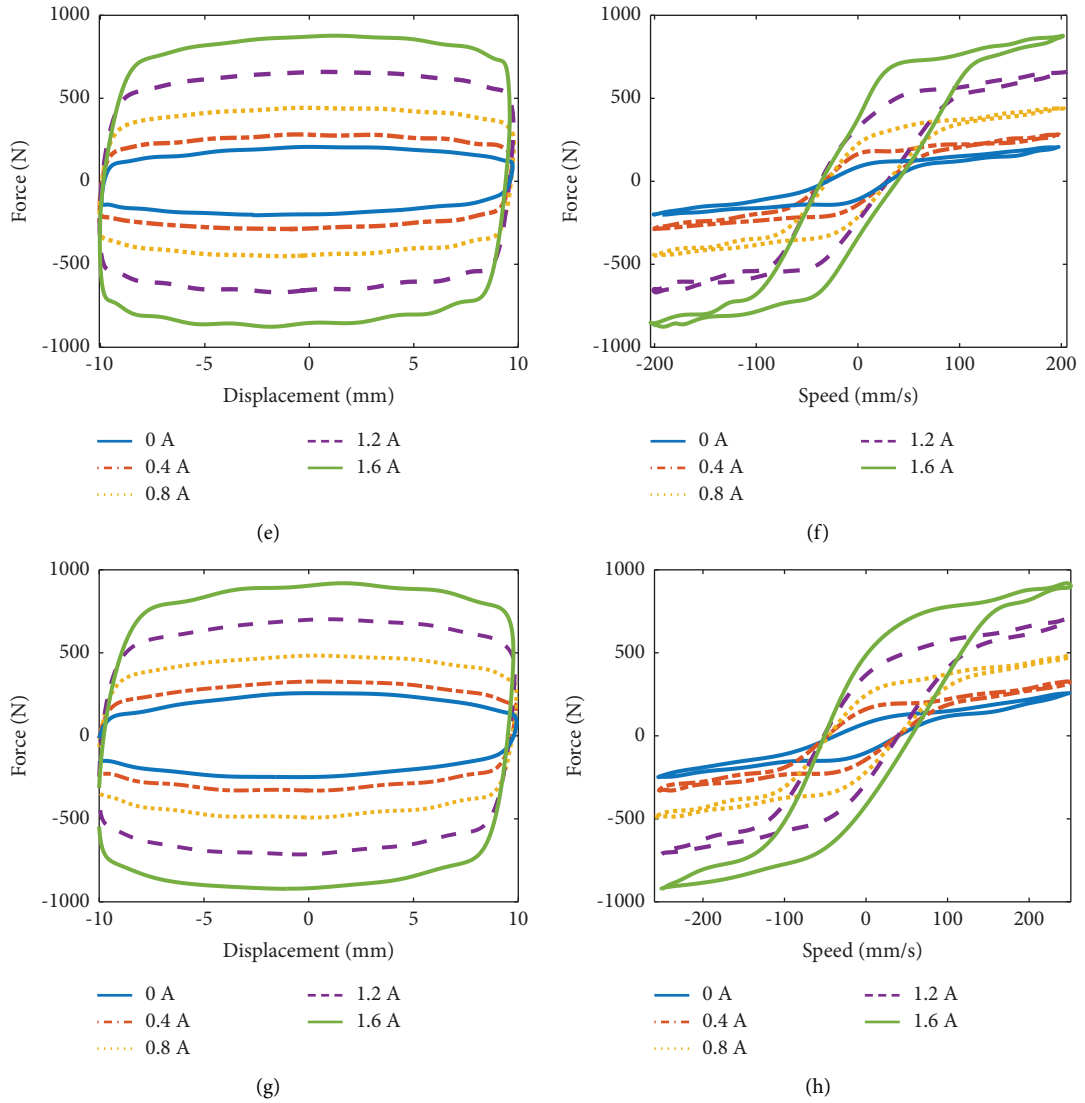

Figure 4: MR damper test results. (a) Force-displacement curve (1.6 Hz). (b) Force-speed curve (1.6 Hz). (c) Force-displacement curve (2.4 Hz). (d) Force-speed curve (2.4 Hz). (e) Force-displacement curve (3.2 Hz). (f) Force-speed curve (3.2 Hz). (g) Force-displacement curve (4 Hz). (h) Force-speed curve (4 Hz).

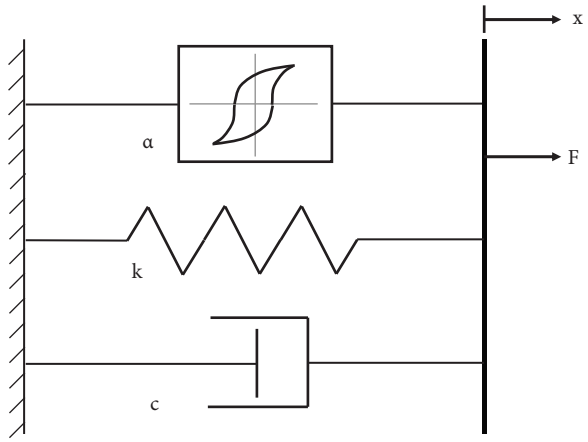

Figure 5: Hysteresis model.

Table 1: Parameter fitting values of a hyperbolic tangent model.

I	c_0	k_0	α	β	δ	f_0
0	0.000449	0.002172	0.08836	0.08409	1.137	0.00062
0.4	0.000539	0.001489	0.1675	0.07201	1.0856	−0.00038
0.8	0.000898	0.00126	0.29	0.06225	0.8572	−0.00257
1.2	0.001184	0.000211	0.4992	0.0431	0.678	−0.0003
1.6	0.001217	0.000249	0.7658	0.03119	0.607	0.00506

$$\begin{aligned} F = {} & 0.005 + (0.0005 \cdot I + 0.0004) \cdot \dot{x} + (-0.0015 \cdot I + 0.0022) \cdot x \\ & + \left(0.2061 \cdot I^2 + 0.0919 \cdot I + 0.0908\right) \cdot \tanh\left((-0.0337 \cdot I + 0.0849) \cdot \dot{x} + (-0.3669 \cdot I + 1.1665) \cdot \operatorname{sign}(x)\right), \end{aligned} \tag{3}$$

where units of the speed $\dot{x}$, displacement x, and damping force F are mm/s, mm, and kN, respectively.

The damping model can be established with MATLAB with the above equations, and modeling results are compared with the experimental results, as shown in Figure 6. Both inputs are measured from the test bench surface. Both sets of results exhibit good agreement with the force-displacement and force-speed loops while jerks are observed due to poor flow of the MR fluid under the influence of a strong magnetic field, leading to the formation of cavities in the damper (Figure 6(b) shows this occurrence in the 1.6A case). These inconsistencies are not accurately reproduced in the model loops. Despite the potential for damping control errors, they are acceptable as they only occur at the highest current and relatively low-frequency conditions.

To verify the model, a 2.4 Hz harmonic signal is given as the input in MATLAB. Figure 7 shows the results in comparison with the experiment. Although the displacement data are not exactly coincident because of the mechanical errors of the test bench during vibration, all results still have good agreement for the force-displacement and force-speed loops. Consequently, the mathematical model can predict the MR damper force in a satisfactory level.

2.3. Mathematical Modeling of the Seat Suspension. The seat suspension and the passenger on it can be simplified to the model as shown in Figure 8 [18]. m_b and m_z represent the masses of the human and the seat. k_{ep} and c_{ep} are the equivalent stiffness and damping coefficients of the human body. k_{es} and c_{es} are the equivalent stiffness and damping coefficients of the seat suspension.

The c_{es} value can be calculated by the MR damper model shown above with the MR damping force. The air spring force F_E is given by

$$\begin{aligned} F_E &= \mathrm{PA} \\ &= \frac{P_0 V_0^n A}{(V_0 + Ax)^n}, \end{aligned} \tag{4}$$

where P and A are the air pressure and effective area of the air spring. P_0 and V_0 are the pressure and volume of the air spring at the initial moment. According to Figure 1(b), the air spring is not installed vertically, which means the air spring force cannot act on the top plate directly. During the suspension working, the angle φ and the direction of the air spring force acting on point E are changing. Hence, in order to reduce the dynamic model of seat suspension to Figure 8, the equivalent spring force F_{se} acting vertically on the suspension top plate is calculated with the air spring force and a changing function related to the changing angle σ and φ.

$$F_{se} = F_E \cdot \frac{(l_1 \cos\sigma \sin\varphi \mathrm{f} + l_2 \cos\sigma \cos\varphi)}{l_1 \cos\sigma f}, \tag{5}$$

where f is the rolling friction coefficient at sliders B and D and $((l_1 \cos\sigma \sin\varphi \mathrm{f} + l_2 \cos\sigma \cos\varphi)/l_1 \cos\sigma \mathrm{f})$ reflects the nonlinear structures of suspension, which can be generated according to force and moment balance on suspension beams 1 and 2. In the above equations, all the required parameters can be measured from seat suspension or read on specification, as shown in Table 2. Additionally, m_b is the average adult male weight, and it is 70 kg according to adult male body size. The curve of F_{se} is shown in Figure 9. Then, the equivalent stiffness k_{es} is equal to the slope of the curve of F_{se}.

The accuracy of the model is verified by applying various harmonic signals with different frequencies in MATLAB. The simulated results are compared to the experimental data, as depicted in Figure 10. For the excitation frequency of 1.8 Hz, which is close to the resonant frequency of the seat suspension, slight differences are observed between the model and experimental results for seat displacement and relative displacement of the seat suspension. These disparities can be attributed to initial conditions and steady-state vibration of the test bench. The difference in seat displacement is approximately 7.8%, while the difference in relative displacement of the seat suspension is approximately 7.6%.

Figure 11 shows the results when the excitation frequency is 4 Hz, which is a relatively high frequency for human bodies. It is observed that the difference in relative displacement of the seat suspension is small, while the difference in the seat displacement is relatively large. The red box in Figure 11(a) shows some abnormalities of the test bench during vibration, causing the curve to go up and down. This scenario can also be depicted by the

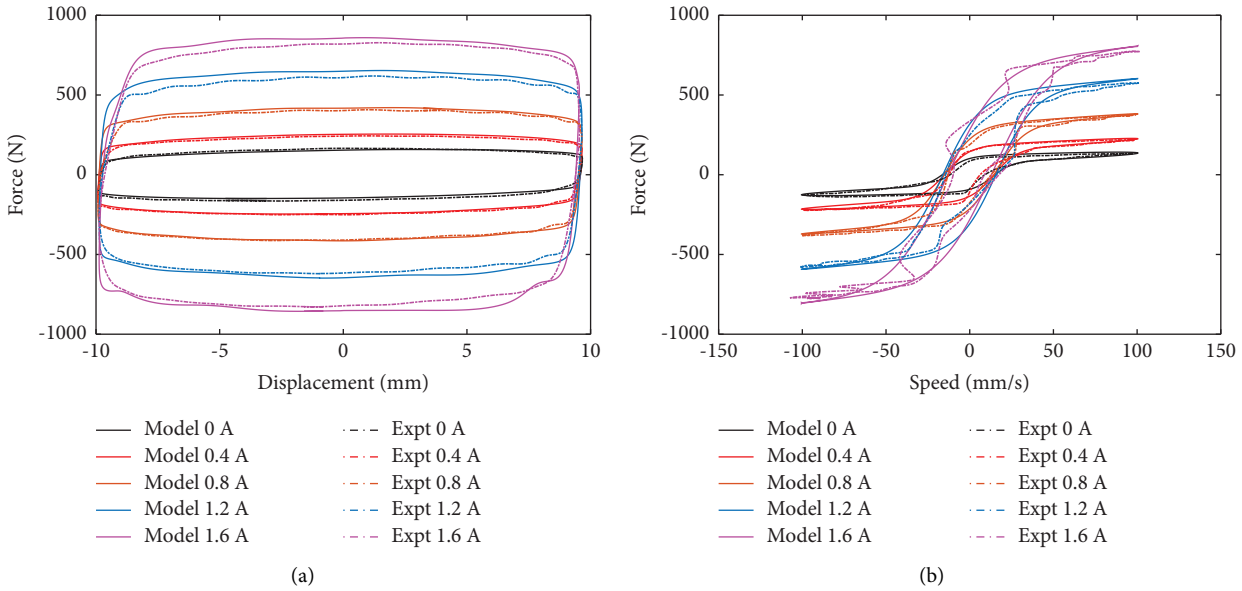

Figure 6: Results comparison for the experimental excitation signal. (a) Force-displacement curve (1.6 Hz). (b) Force-speed curve (1.6 Hz).

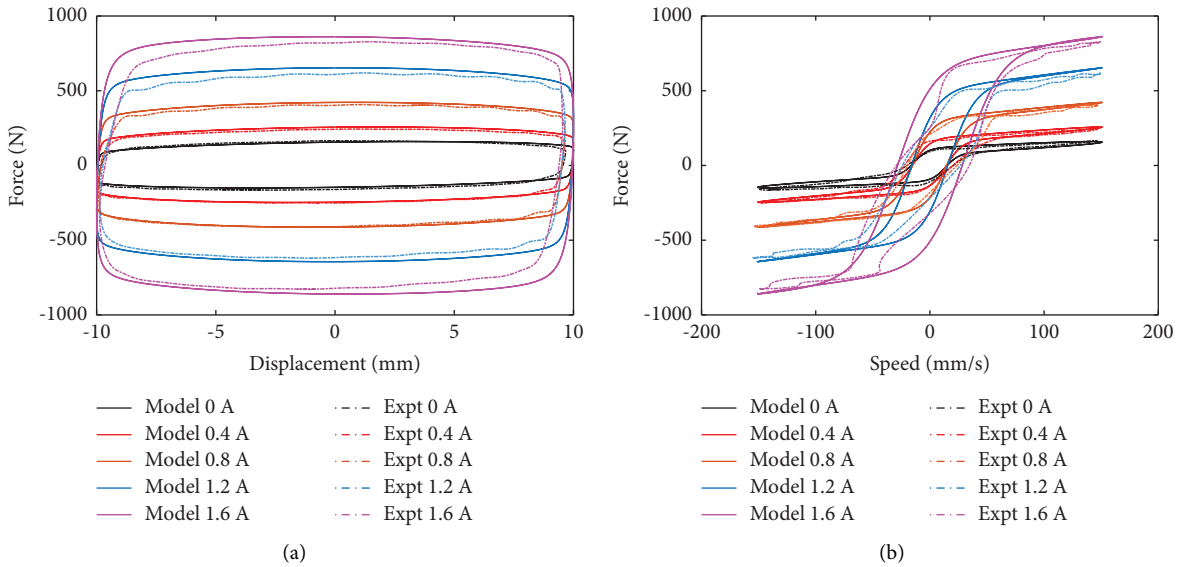

Figure 7: Results comparison for the digital excitation signal. (a) Force-displacement curve (2.4 Hz). (b) Force-speed curve (2.4 Hz).

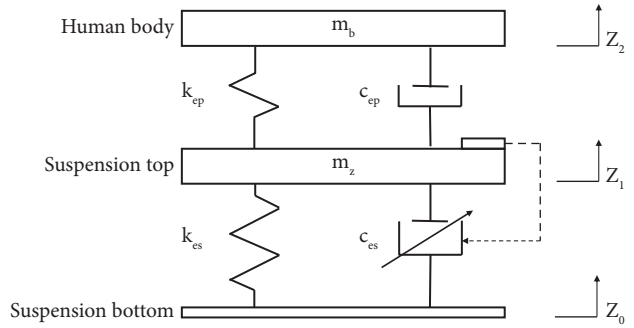

Figure 8: Seat suspension model.

Table 2: Parameters of seat.

Parameter	Data
l_1 (m)	0.17
l_2 (m)	0.17
l_3 (m)	0.004
l_4 (m)	0.007
l_5 (m)	0.21
l_6 (m)	0.12
m_z (kg)	18
A (m^2)	3.972×10^{-3}
H_0 (m)	0.06
n	1.38
γ (°)	40.5
H (°)	31
V_0 (m^3)	6.725×10^{-4}
F	0.05
m_b (kg)	70
P_0 (MPa)	0.35

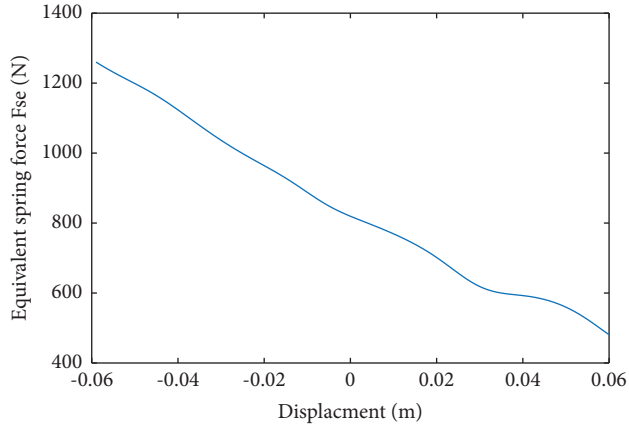

Figure 9: Equivalent spring force curve.

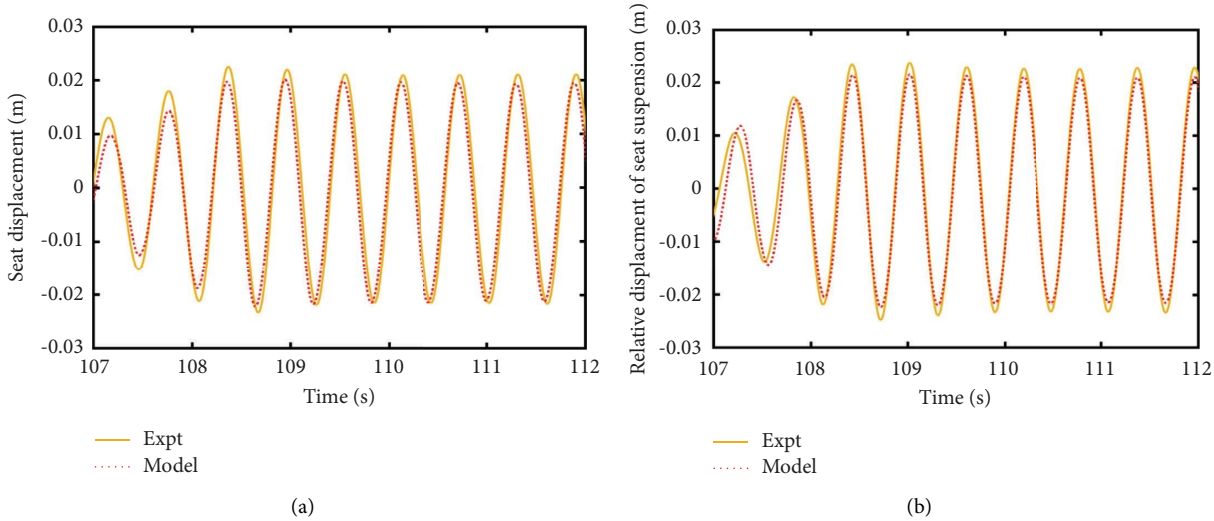

Figure 10: Model results comparison at 1.8 Hz. (a) Seat displacement (1.8 Hz). (b) Relative displacement of seat suspension (1.8 Hz).

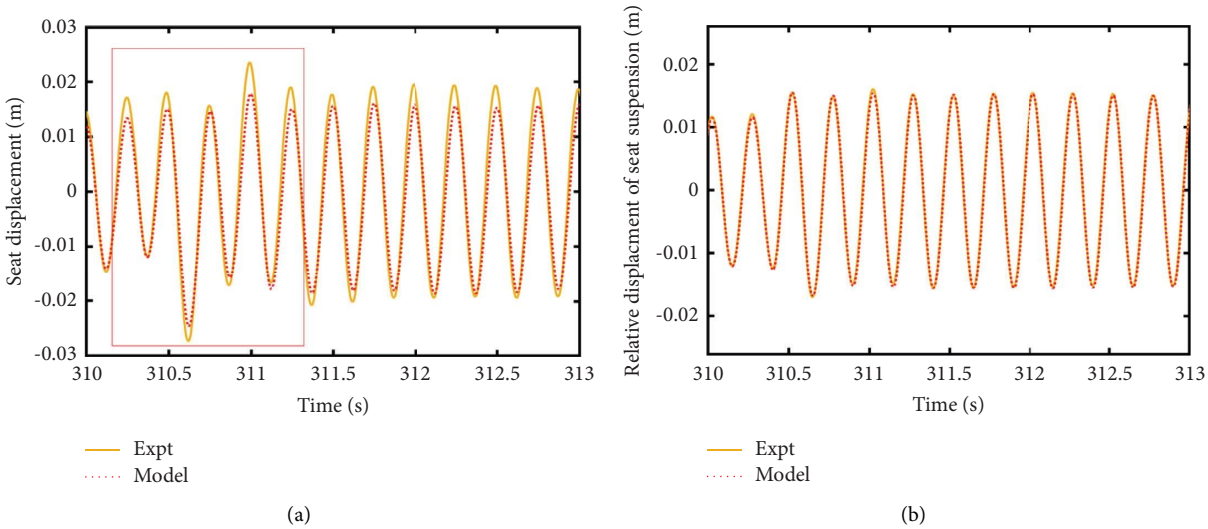

Figure 11: Model results comparison at 4 Hz. (a) Seat displacement (4 Hz). (b) Relative displacement of seat suspension (4 Hz).

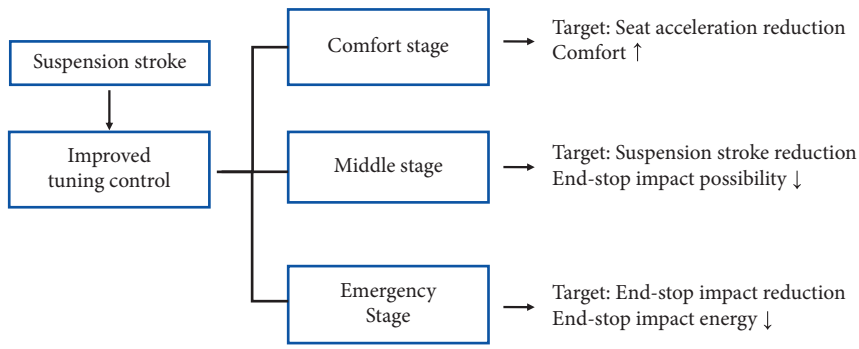

Figure 12: Three control stages of improved tuning control.

MATLAB model. Hence, the accuracy of this model is considerably enough to reflect the behavior of the seat suspension, and the model can be used to design the further control algorithm.

3. Control Strategy Design

3.1. Block Diagram of the Controller. To reduce vibration and avoid end-stop impacts, an improved tuning control strategy based on single-sensor control [36] is selected for this study. The strategy is divided into three control stages in accordance with the relative displacement of the seat suspension, as shown in Figure 12.

If the relative displacement of the seat suspension is lower than the setting threshold, the control strategy based on single-sensor control is in the comfort stage, which could provide a good vibration attenuation performance. Furthermore, when the suspension is approaching the maximum and minimum stroke, a high damping force should be provided to reduce the relative displacement and avoid end-stop impacts for the emergency case. In the middle stage, the vibration amplitude is relatively high so that the damping force will increase smoothly according to the relative displacement of the suspension and attempt to reduce the suspension stroke slowly back to the comfort stage. The block diagram of this control strategy is shown in Figure 13. When the seat suspension is working, the control stages will be adjusted by controller 1 according to the data measured by sensors, and the damping force will be given to the MR damper inverse model by controller 2 according to the logic of control stages. Then, the desired current will be calculated and applied to the MR damper, and as a result, the MR damper can adjust the damping according to different working conditions.

3.2. Comfort Control with Frequency Selector. The comfort control strategy is used to reduce seat acceleration, which can make people feel comfortable according to ISO 2631 [37]. In order to analyze the vibration patterns of general suspension, in this part, a normal seat suspension is reduced to a single degree of freedom system, and the transfer function can be written as follows:

$$G(s) = \frac{k + \mathrm{Cs}}{ms^2 + k + \mathrm{Cs}}, \tag{6}$$

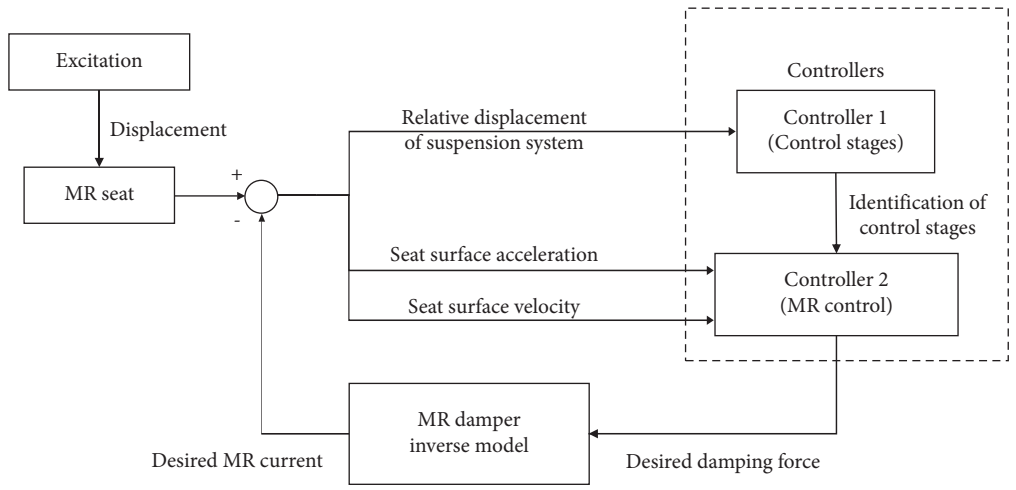

Figure 13: Block diagram of the improved tuning control.

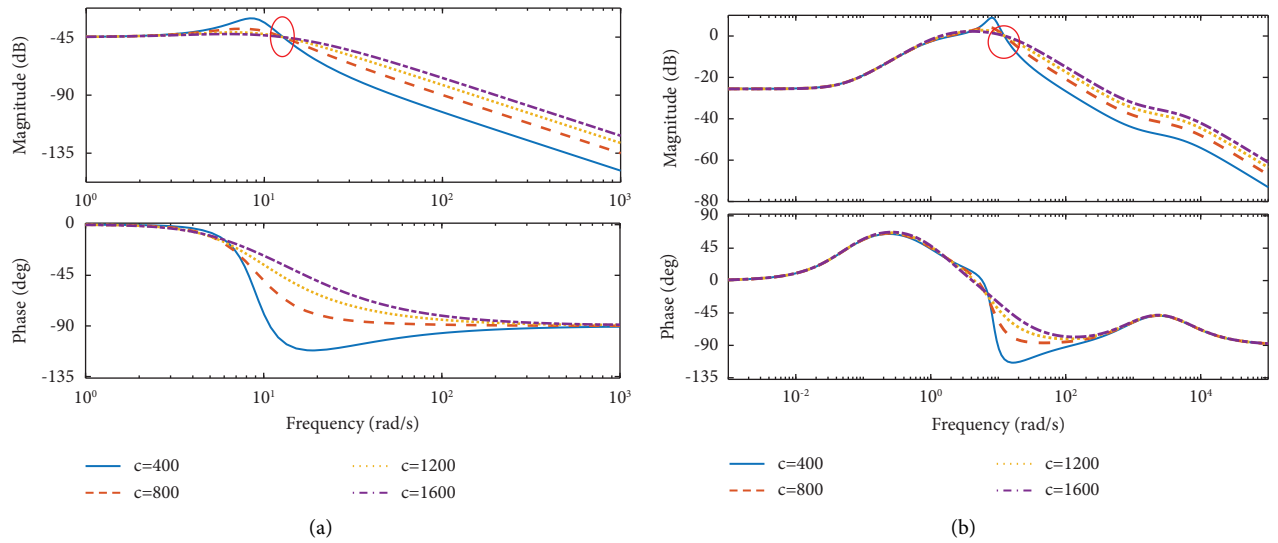

Figure 14: Bode diagram of vibration system. (a) Bode diagram of 1-DOF system. (b) Bode diagram of 2-DOF system.

where k, m, and C are the stiffness, mass, and damping of the system. Therefore, this kind of system follows the same rule with harmonic excitation acting on the bottom, as shown in Figure 14(a).

The vibrating amplitude has different trends with the damping C changing on both sides of the point (i.e., turning point) in the red circle in Figure 14(a). When the vibration frequency is smaller than the turning point, the amplitude is reduced when C increases, and when the vibration frequency is larger than the turning point, the amplitude is increased when C increases. This conclusion also can be extended to 2-DOF systems such as the human-seat suspension system, which is shown in Figure 14(b). Therefore, different damping values are needed with different vibration frequencies to achieve good vibration attenuation in place of the fixed value to dampen the system. A frequency selector proposed by Savaresi and Spelta [36] in single-sensor control is used to meet this requirement, which is given by

$$\begin{cases} c_d = c_{\max}, & \text{if } \left(\ddot{z}^2 - a^2\dot{z}^2\right) \le 0, \\ c_d = c_{\min}, & \text{if } \left(\ddot{z}^2 - a^2\dot{z}^2\right) > 0, \end{cases} \tag{7}$$

where c_d is the target damping of the seat suspension; $\ddot{z}$ and $\dot{z}$ are the acceleration and velocity of the suspension top plate; and a is set according to the resonance frequency q (rad/s) of the seat system, which is defined as $a = \sqrt{2}q$. The q term can be experimentally measured. In this study, $q \approx 11.3$ rad/s (i.e., 1.8 Hz), and then, a ≈16 rad/s.

From equation (7), the maximum damping and minimum damping are applied to the seat suspension by comparing the vibration frequency of the suspension and the target point a. However, huge jerks are caused by the binary logic of this control strategy during applications, as shown in Figure 15.

The acceleration curve simulation of the seat with random road excitation via equation (7) shows some time regions reflecting the damping force switches quickly when

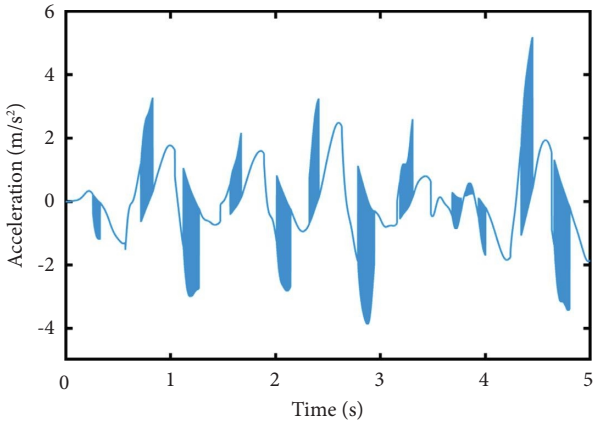

Figure 15: Simulation results of equation (7) control.

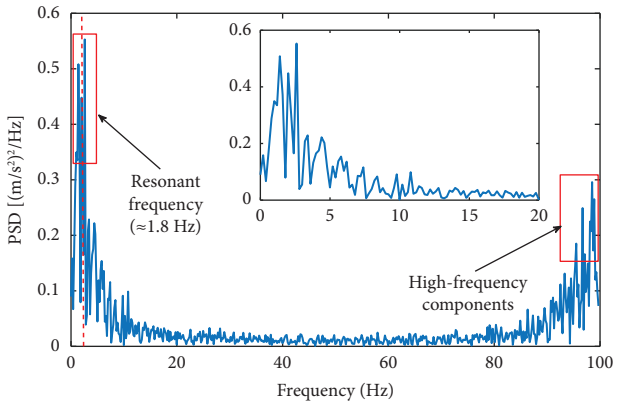

Figure 16: Simulation results of equation (7) in the frequency domain.

the frequency selector $(\dddot{z}^2 - a\dot{z}^2)$ changes and crosses the zero. Figure 16 gives the correlated power spectral density (PSD) function in the frequency domain.

Figure 16 gives a sense of the jerks in the PSD plot. The high-frequency components (noted in the red box in Figure 16) could cause the low-frequency some jerking effects, especially the resonant frequency [34]. The jerks in the high frequency may not appear in reality circumstances, but the impact will cause the binary control logic and make passengers feel uncomfortable, which has been discussed by paper [34]. Hence, an analytic continuous function is employed to make the damping force change smoothly, which is given as follows:

$$\begin{cases} c_d = c_{\min}, & \text{if } \left(\dddot{z}^2 - a^2\dot{z}^2\right) > 0, \\ c_d = c_{\min} + K\left|\dddot{z}^2 - a^2\dot{z}^2\right|, & \text{if } \left(\dddot{z}^2 - a^2\dot{z}^2\right) \le 0, \end{cases} \tag{8}$$

where the K is a constant gain. For this control strategy, the damping force is related to the frequency selector, and the jerks can be reduced with the continuously changing damping force, as shown in Figure 17.

By comparing with the original logic in equation (7), the improvement of the control strategy has relatively poor vibration attenuation performance. It is observed that there is no obvious jerk appearing during the simulation. This can

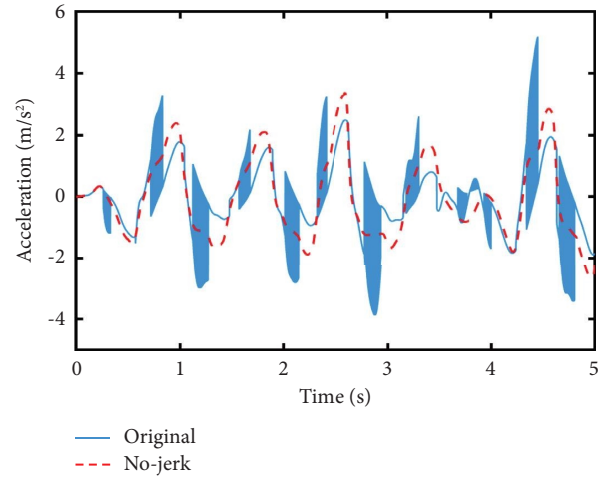

Figure 17: Simulation results comparison.

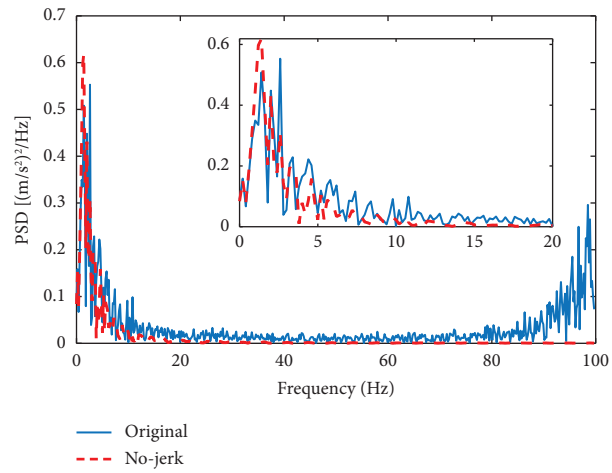

Figure 18: Simulation results in the frequency domain.

be also found in the PSD plot in the frequency domain, as shown in Figure 18. The high-frequency components are reduced well in the red curve of improving strategy.

3.3. End-Stop Impact Countermeasures. The main control target of the middle stage and emergency stage is the reduction of the relative displacement of the seat suspension. The comfort control strategy can provide a suitable damping force for acceleration attenuation, though it cannot deal with emergencies appearing during driving such as a sharp shock caused by a bump or pit in the road. The frequency selector will choose a low damping force when the seat vibrates at a relatively high frequency. End-stop impacts may easily happen at this time if there are terrible shocks acting on the seat suspension. Additionally, the end-stop impacts will easily happen when the seat height is set too high or low so that there is not enough space for vibration. Hence, in the middle stage, the control strategy should keep reducing the relative displacement of the seat suspension to avoid end-stop impacts. To ensure good vibration performance without the serious jerks shown in Section 3.2, the damping force is

designed to rise smoothly with the suspension stroke, and it should be at a maximum if the suspension is too close to the top or bottom limits.

An exponential function $E^{q(h-d_m)}$ is added into equation (8) to meet the above requirements, and this is shown as follows:

$$\begin{cases} c_d = c_{\min} + K\left|\varepsilon'\right|, & \text{if } \varepsilon' \le 0, \\ c_d = c_{\min}, & if\ \varepsilon' > 0, \\ \varepsilon' = \left(\ddot{z}_1^2 - b\dot{z}_1^2\right), & \\ b = a^2 + E^{q\left(h-d_m\right)}, & b < b_m, \end{cases} \tag{9}$$

where d_m is the threshold of the comfort stage, b_m is the maximum value of b, h is the suspension stroke from the neutral position, and the frequency selector is improved to ε'. E and q are constant gains for adjusting the raising speed of b. In this control strategy, the comfort stage is combined with the middle stage using the function $E^{q(h-d_m)}$. The $E^{q(h-d_m)}$ curve is presented in Figure 19. When $h < d_m$, the value of $E^{q(h-d_m)}$ is extremely close to zero so that $b \approx a^2$, and the damping force control can follow the nearly same rule as equation (8). At this time, the control strategy is in the comfort stage. When $h > d_m$, this value for $b = a^2 + E^{q(h-d_m)}$ will rise quickly; therefore, the frequency selector $\varepsilon' = (\ddot{z}_1^2 - b\dot{z}_1^2)$ will preserve $\varepsilon' \le 0$. Hence, a large damping force will be experienced by the seat suspension, the stroke will be reduced, and the control strategy will be in the middle stage.

Simulation results for middle-stage control under random road excitation are presented in Figure 20. It can be observed that both of the governing equations (equations (8) and (9) have similar results in Figure 20(a), while several small jerks appear at peaks of equation (9) curve. These jerks are caused by the damping force raising when the relative displacement of the seat suspension is larger than the threshold of the comfort stage. Otherwise, the suspension stroke (relative displacement of seat suspension) of equation (9) goes lower than that of equation (8) as shown in Figure 20(b).

In the emergency stage, the seat vibration amplitude is relatively large, and the suspension stroke occupies a large proportion of all available strokes. The maximum damping force should be given at this time to dissipate the vibration energy and avoid end-stop impacts. According to all the control logic above, the study proposed a modified mutistage control strategy, which can be defined as follows:

$$\begin{cases} c_d = c_{\min}, & \text{if } [\varepsilon' > 0 \cap h < d_d], \\ c_d = c_{\min} + K\left|\varepsilon'\right|, & \text{if } [\varepsilon' \le 0 \cap h < d_d], \\ c_d = c_{\max}, & \text{if } h \ge d_d, \end{cases} \tag{10}$$

where d_d is the threshold of middle-stage control and $c_{\max}$ is the MR damping with the maximum working current, which is 2A in this study. The d_d is designed to dissipate all the vibration energy with the maximum seat velocity and maximum operating current, and it can be calculated roughly by

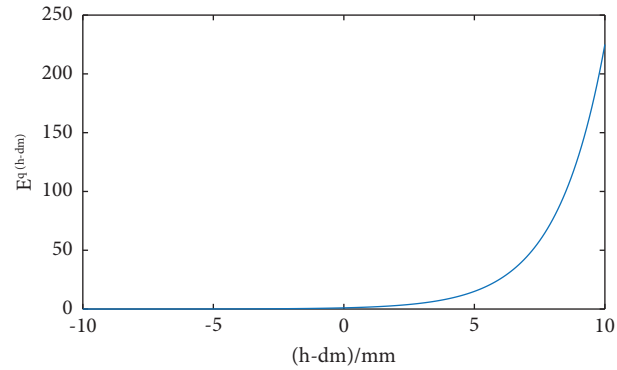

Figure 19: The curve of $E^{q(h-d_m)}$.

$$\begin{cases} \dfrac{v_m^2 \cdot m}{F_{se} + F_{de} - mg} = 2\left|l_m - d_d\right| (v_m < 0), \\ \dfrac{v_m^2 \cdot m}{F_{se} + F_{de} + mg} = 2\left|l_m - d_d\right| (v_m \ge 0), \end{cases} \tag{11}$$

where v_m is the maximum seat velocity and l_m is the largest suspension stroke. All the parameters of the control strategy are optimized experimentally, as shown in Table 3.

3.4. Numerical Simulation Results and Analysis. Numerical simulations based on the mathematical model in Section 2 are conducted using MATLAB/Simulink to evaluate the control performance of the MR seat suspension. Three types of excitation, namely harmonic, bump, and random road excitation, are chosen to simulate different working conditions of commercial vehicles. In order to get the correct excitation acting on seat suspension, a 1/2 truck dynamic model is used as a filter as shown in Figure 21. Three types of excitation above will act on the tires of this model, and target signals can be measured from the cab part. To prove the effectiveness of the damping variability, some control strategies of the seat suspension are compared, which are noted as follows:

(1) Passive seat case. $I = 0.9$A is set as the current input to represent a passive suspension with constant damping. The seat performance is roughly similar to the same seat with the original passive damper.

(2) Improved tuning control case. The damping is controlled by the MS strategy in this case.

(3) Skyhook control case. The damping is controlled by the Skyhook strategy in this case. $I = 0$A and $I = 2$A are set as the minimum and maximum damping in this control logic.

(4) Single-sensor control case. The damping is controlled by the original single-sensor control strategy in this case. The parameters for the frequency selector are the same as those for improved tuning control, in which $I = 0$A and $I = 2$A are set as the minimum and maximum damping in this control logic.

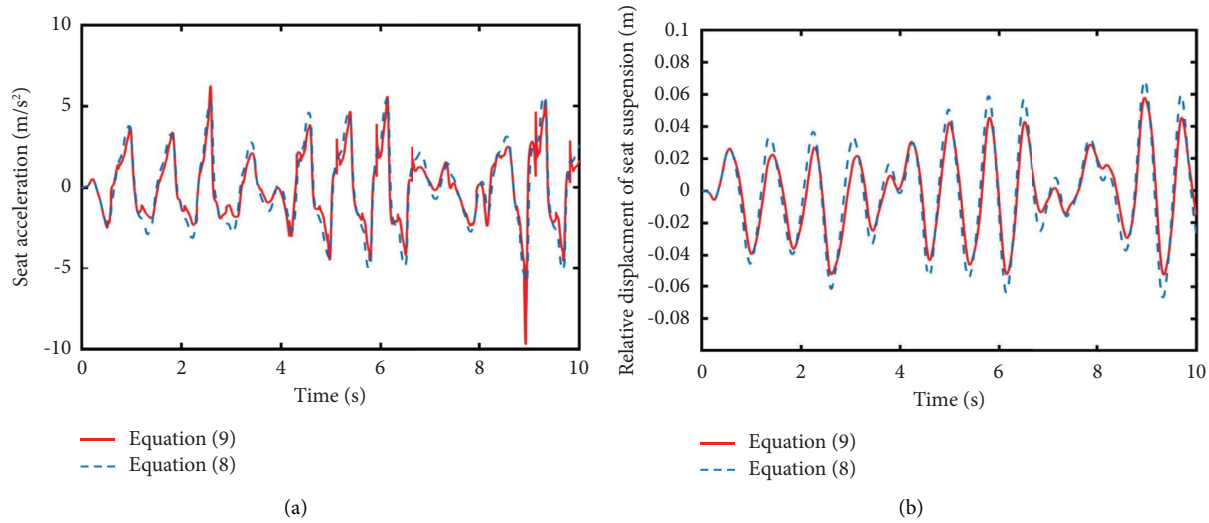

Figure 20: Simulation results under random road excitation in comparison with equations (8) and (9). (a) Acceleration time history. (b) Relative displacement of seat suspension time history.

Table 3: Parameters of the improved tuning control strategy.

Parameter	Value
d_m (mm)	10
d_d (mm)	48
E	2
K	300
q	3500
a	11.3

3.4.1. Simulation of Harmonic Excitation. Harmonic signals simulation is provided to investigate the performances of the frequency selector to ensure the control logic performance at a specific frequency. Two typical frequencies are chosen as 1.8 Hz and 4 Hz. These two cases reflect two different conditions during seat suspension work in that the seat resonant conditions at relatively low and high frequencies affect driver health and ride safety performance.

The detailed simulation is shown in Figures 22 and 23. The passive seat case is compared with the other three control strategies (improved tuning control, Skyhook, and single-sensor). Apparently, the three control strategies have better performance, and the seat acceleration amplitudes are largely reduced by approximately 30%. The single-sensor and skyhook cases have obvious jerks in each period caused by binary control logic, while the improved tuning control has better performance. Consequently, the improved tuning control is effective to improve the jerk effect. In addition, the three control strategies have similar performance compared with the passive seat case, as shown in Figures 22(b) and 22(c). This could be the reason for improved tuning control and single-sensor control having similar control logic to Skyhook control when the seat vibration frequency is lower than the frequency set in the frequency selector.

In the 4 Hz case, as shown in Figure 23, the vibration control performance is also improved in the Skyhook, MS, and single-sensor cases compared with the passive seat case. However, the problem of jerking becomes worse with the frequency rises, and the proposed control maintains a good performance in that no jerks appear in the improved tuning control curve, as shown in Figure 23(a).

The transmissibility defined as the displacement amplitude ratio of the seat to the floor for each case is shown in Table 4. The Skyhook and single-sensor control have similar transmissibility in comparison with the passive seat control. The transmissibility of the improved tuning control case remains the lowest at both 1.8 Hz and 4 Hz, indicating the best vibration attenuation performance.

3.4.2. Simulation of Bump Excitation. Simulations with bump displacement excitation are conducted to evaluate the instantaneous response performance of the seat suspension. The results are presented in Figure 24. From the general view of the relative displacement, as shown in Figure 24(a), the three control strategies cases have much smaller oscillations than the passive cases. This means that there are fewer possibilities for end-stop impacts using the three control strategies. In Figure 24(a), the red box has no effective performance of all control schemes when the shock acts on the seat suspension. The suspension stroke becomes larger than the threshold in the proposed control quickly, so it most quickly reduces the relative displacement, as shown in the red dotted box. There is a 46.3% improvement at peak compared with the passive control seat, which is also slightly better than the single-sensor case and much better than the Skyhook case. Then, the improved tuning control goes back to the comfort stage, and the reducing speed of the suspension stroke slows down, as shown in the black and black dotted boxes, which is expected according to the design discussion in Section 3.3. In the meantime, the Skyhook case and single-sensor cases attenuate faster than the passive seat and improved tuning control cases.

The acceleration response is shown in Figure 24(c). There is a signal jerk in the improved tuning control response, indicating that the damping force increases at this

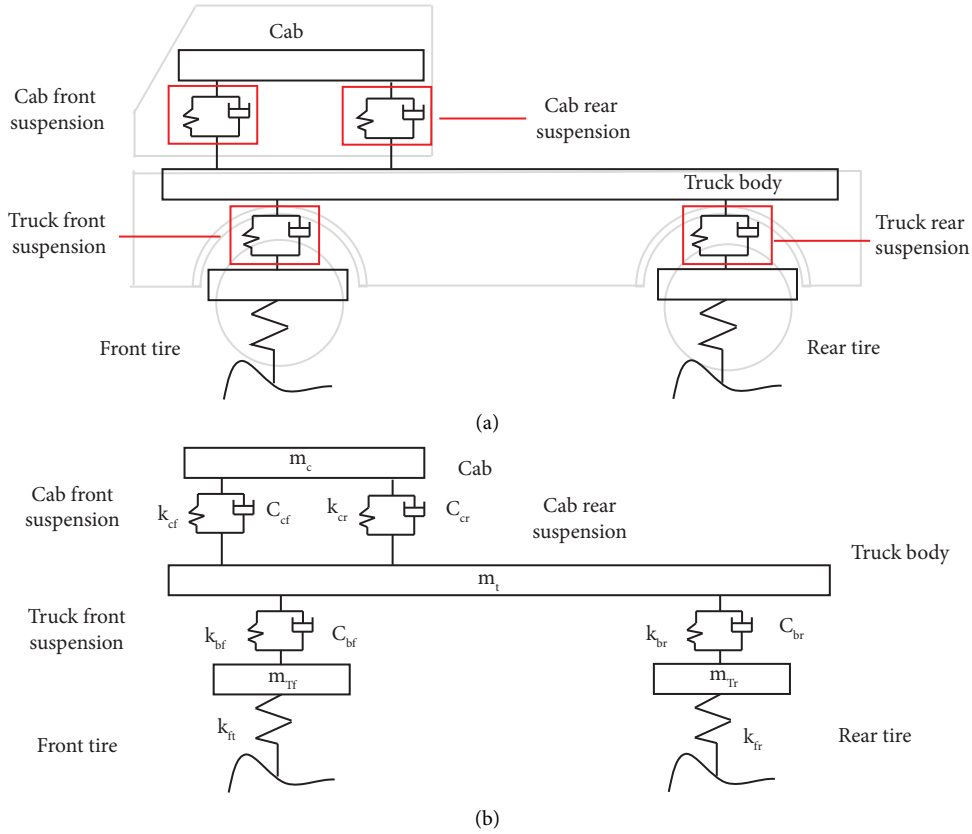

FIGURE 21: The ½ truck model. k_{cf} & c_{cf}: stiffness and damping of cab front suspension, k_{cr} & c_{cr}: stiffness and damping of cab rear suspension, k_{bf} & c_{bf}: stiffness and damping of truck front suspension, k_{br} & c_{br}: stiffness and damping of truck rear suspension, k_{ft} & k_{fr}: stiffness of front and rear tires, m_c: mass of cab, m_t: mass of truck body, m_{Tf} & m_{Tr}: mass of front and rear tires.

time, as shown in the red box, which is consistent with the previous conclusions as designed in Section 3.3. Moreover, the single-sensor case still has the jerk problem during the vibration, as shown in the green line in Figure 24(c), while the MS and Skyhook control cases do not have this issue, demonstrating the improvement of these two control schemes, especially the benefit of improved tuning control.

3.4.3. Simulation of Random Road Excitation. The comprehensive performance of the seat suspension can be evaluated with random road excitation. The results are shown in Figure 25. The acceleration and displacement responses of the seat in Figures 25(a) and 25(b) are illustrated that the seat vibration is reduced with three control strategies in comparison with the passive control seat. The improved tuning control has the best performance among all cases. Although the single-sensor case shows similar results to the improved tuning control case, it still has a relatively serious jerk problem, as shown in Figure 25(a). This can be also observed in the PSD plot of the seat suspension, as shown in Figure 25(d). The improved tuning control cases have a 40% reduction compared with the passive control seat case around the dominant frequency of the vibration at 1.8 Hz. Moreover, the suspension stroke is larger than 0.06 m in the passive control seat case, as shown in the red box in Figure 25(c), which is the upper limit of the suspension stroke. At this time, end-stop impacts appear and the proposed has the best performance of suspension stroke attenuation, demonstrating that the improved tuning control is the best able to reduce the possibility of end-stop impacts among all control schemes.

An ISO 2631 [36] standard is used to evaluate the comfort of the seat suspension in this study, which uses the frequency weighted root mean square (Aw) of seat acceleration to evaluate the ride comfort of drivers. Additionally, seat displacement can affect the driver's ride performance, while the relative displacement of the seat suspension can be used as an index to evaluate the possibility of end-stop impacts. Therefore, the RMS values of these two indices (RMS rd for relative displacement and RMS *d* for seat displacement) are also used to evaluate the performance of the seat suspension, in which the smaller RMS value is the better performance of the seat suspension. These three indices are compared in all cases in Figure 26. It is observed that the improved tuning control case, represented by the gray bars, has the smallest magnitude in Aw. To compare with the passive control seat case, the improved tuning control case reduces the Aw by 28.4%, the

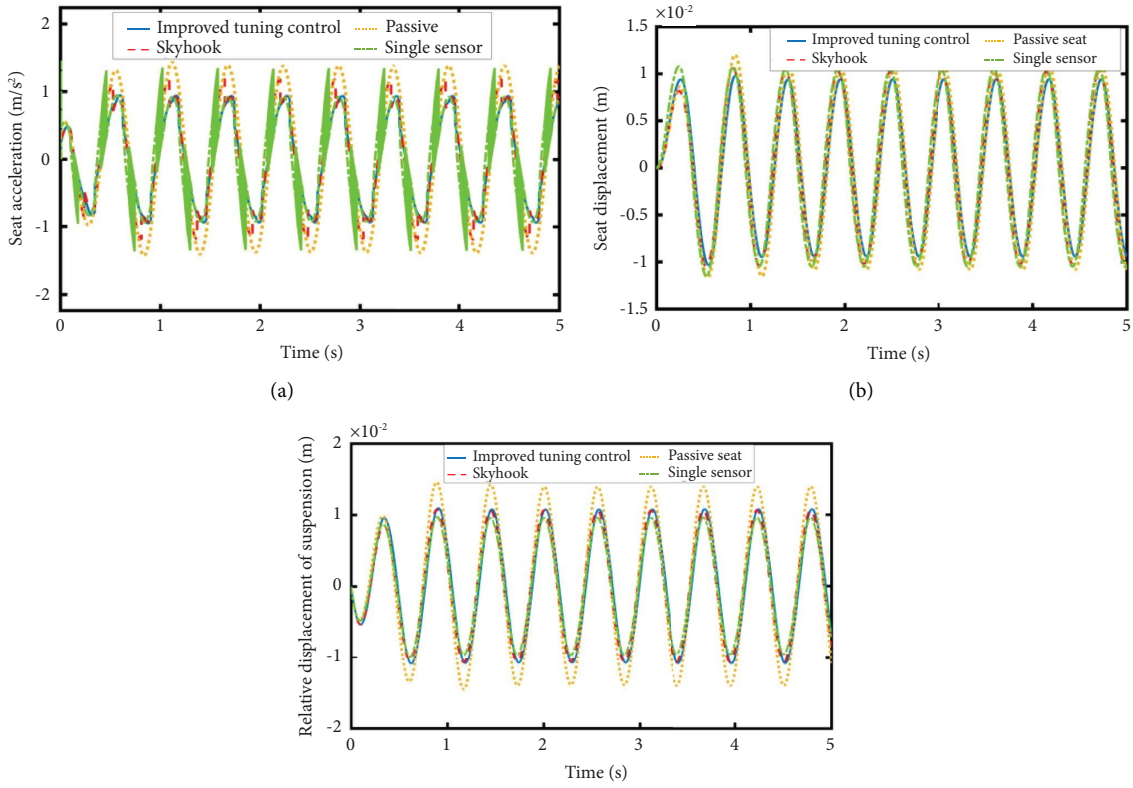

FIGURE 22: Harmonic excitation simulation results at 1.8 Hz. (a) Seat acceleration at 1.8 Hz. (b) Seat displacement at 1.8 Hz. (c) Relative displacement of seat suspension at 1.8 Hz.

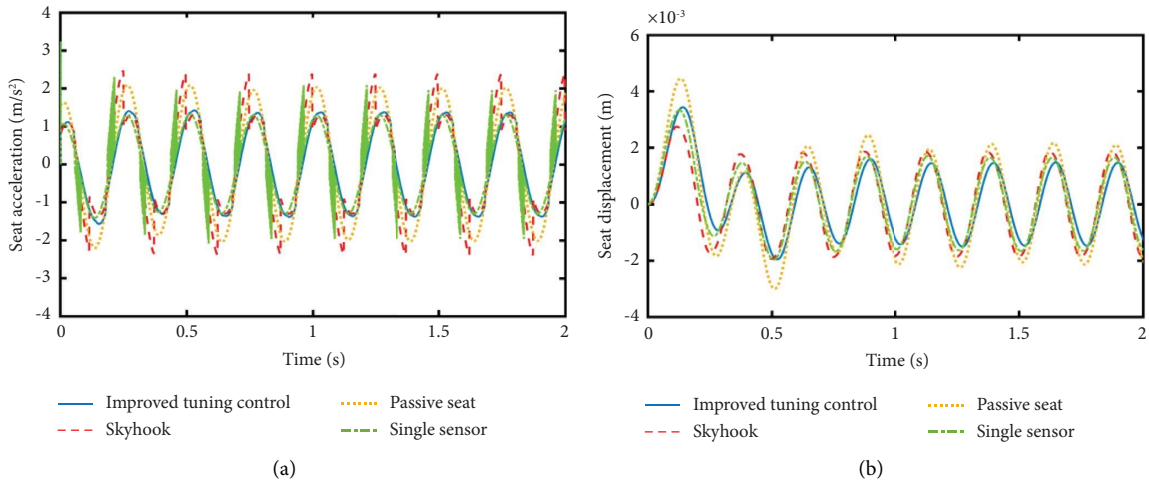

FIGURE 23: Continued.

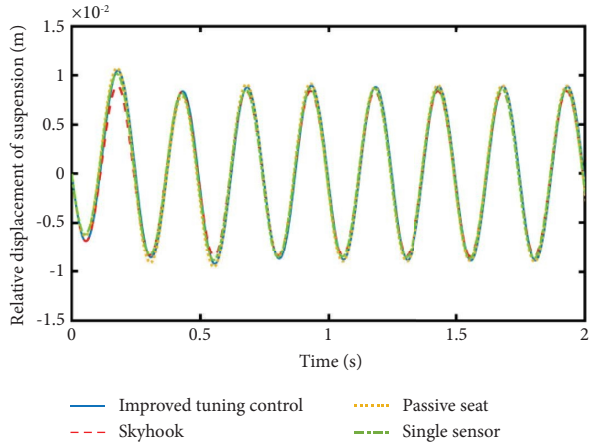

(c)

Figure 23: Harmonic excitation simulation results at 4 Hz. (a) Seat acceleration at 4 Hz. (b) Seat displacement at 4 Hz. (c) Relative displacement of seat suspension at 4 Hz.

Table 4: Transmissibility of simulation at fixed frequency excitation.

	Passive seat		Skyhook		Single sensor		Improved tuning control	
Frequency (Hz)	1.8	4	1.8	4	1.8	4	1.8	4
Transmissibility	1.745	0.267	1.275	0.231	1.262	0.202	1.178	0.179
Improvement	—	—	26.9%	13.5%	27.7%	24.4%	32.5%	33.0%

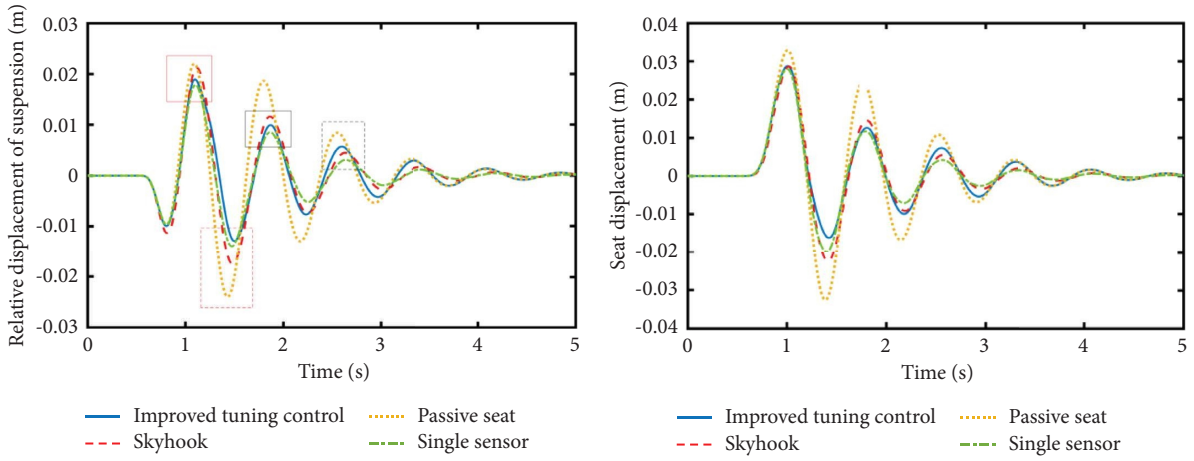

(a) (b)

Figure 24: Continued.

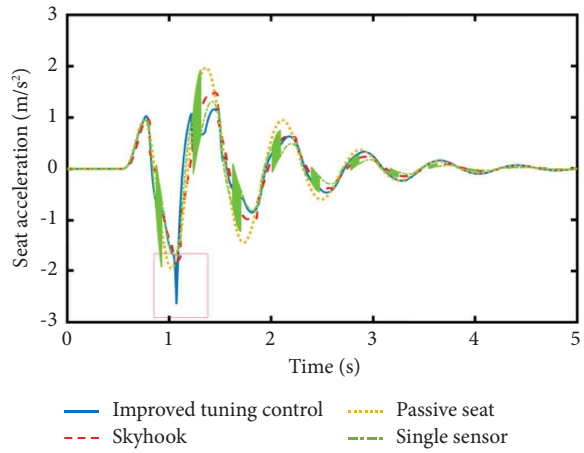

(c)

Figure 24: Bump excitation simulation results. (a) Relative displacement of seat suspension. (b) Seat displacement. (c) Seat acceleration.

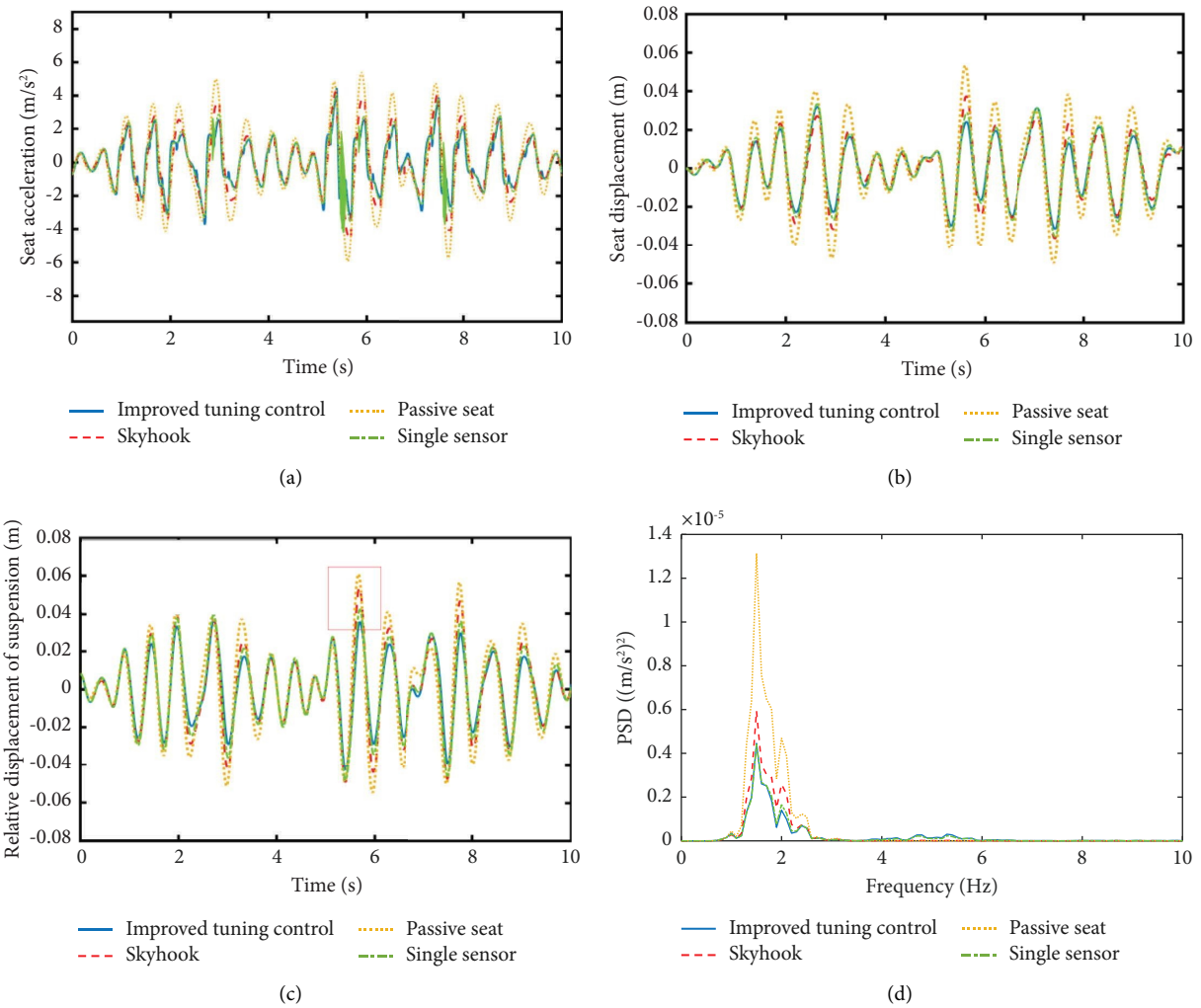

Figure 25: Simulation results for all control schemes under the random road excitation. (a) Seat acceleration. (b) Seat displacement. (c) Relative displacement of seat suspension. (d) Power spectral density of seat suspension.

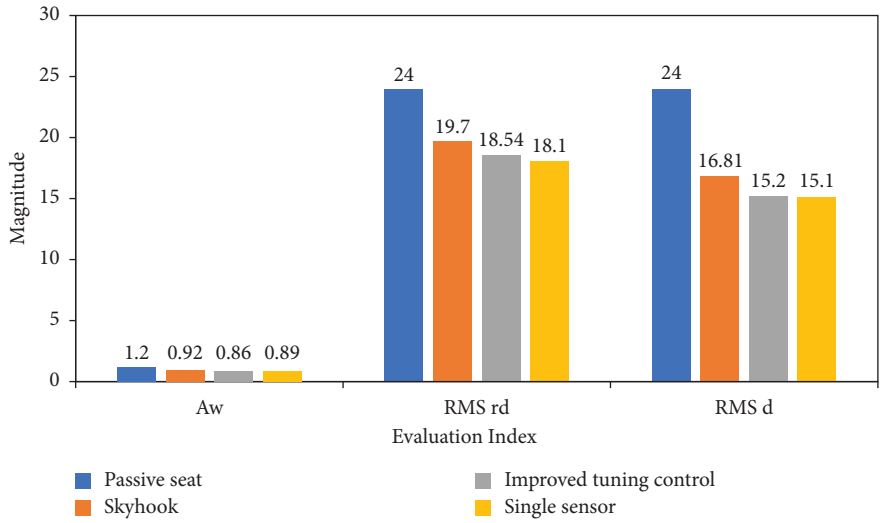

Figure 26: Results comparison of three indices (i.e., Aw, RMS rd, and EMS d).

RMS rd by 22.7%, and the RMS *d* by 36.7%. This is better than the Skyhook case among all indices. Although the single-sensor case has similar results to improved tuning control and has slightly better performances for RMS rd and RMS *d*, it has serious jerk problems and cannot cope with the emergency shock, as stated in Section 3.2 discussion. All the results indicate that the vibration control performance can be largely improved by an MR damper with the proposed strategy in this study.

4. Experimental Evaluation of Seat Suspension

An experiment for seat suspension is organized to verify the conclusions of the analytical simulation. All the simulation and excitation cases are included in the test bench vibration testing.

4.1. Testing Setup. The experiment system is shown in Figure 27. The seat suspension and vehicle seat are attached to a vibration test bench, which can provide vertical excitation controlled by dSPACE and a computer system. A human body mass is loaded onto the seat, and the total weight of them is 88 kg. Two accelerometers (Brüel and Kjær Model 4382) are set on the test bench platform and suspension top plate to measure the acceleration signals. One laser displacement sensor (Panasonic) is set behind the seat to measure the suspension stroke signal. All the signals are transmitted to dSPACE and recorded by a computer. The control strategies manipulate the input current based on real-time analysis results and then pass it through to dSPACE. After that, the current adjusting commands are sent to the amplifier to control the currents and applied to the MR damper. The four cases described in Section 3.4 are examined in this experiment. The response time of the MR damper is around 0.45 s as measured, which can meet the control requirement.

4.2. Analysis of Test Results

4.2.1. Harmonic Excitation Test. In contrast to the simulation, harmonic excitations at several frequencies are used in this test, which are 1 Hz, 1.2 Hz, 1.4 Hz, 1.6 Hz, 1.8 Hz, 2 Hz, 3 Hz, 4 Hz, and 6 Hz. The seat acceleration responses are shown in Figure 28. It is noted that the dynamic performances of the control strategies are improved with the rise of the frequency in comparison with the passive control seat.

The detailed results are shown in Figure 29. It is observed that the seat acceleration is reduced with three control strategies, and the improved tuning control case has the best performance, which can reach the maximum acceleration reduction of approximately 49% at 4 Hz. It is noted that serious jerking problems appear in almost all the results, as shown in the red box in Figure 29(b), which are caused by the mechanical jerking of the test bench and the change in the damping force. Although the improved tuning control can deal with some of these problems to make the curve smoother than other cases, as shown in Figure 29(b), it does not solve all of the problems at the resonant frequency of the system (i.e., 1.8 Hz), as shown in Figure 29(a). Moreover, the seat displacement and suspension stroke are also reduced with the proposed strategy, except the suspension stroke at 1.8 Hz as shown in Figure 29(e). As a result, the improved tuning control case has the best performance, which is slightly better than that of the single-sensor case and much better than that of the Skyhook case. This is similar to the conclusion of the simulation in Section 3.4.1.

The transmissibility of the seat suspension is presented in Figure 30. It can be seen that the improved tuning control case has almost the lowest transmissibility at all frequencies except the resonant frequency. Otherwise, the curve of the single-sensor case has a similar trend to the curve of the improved tuning control. Although the Skyhook case has good performance around the resonance frequency, it has the highest transmissibility after 1.8 Hz

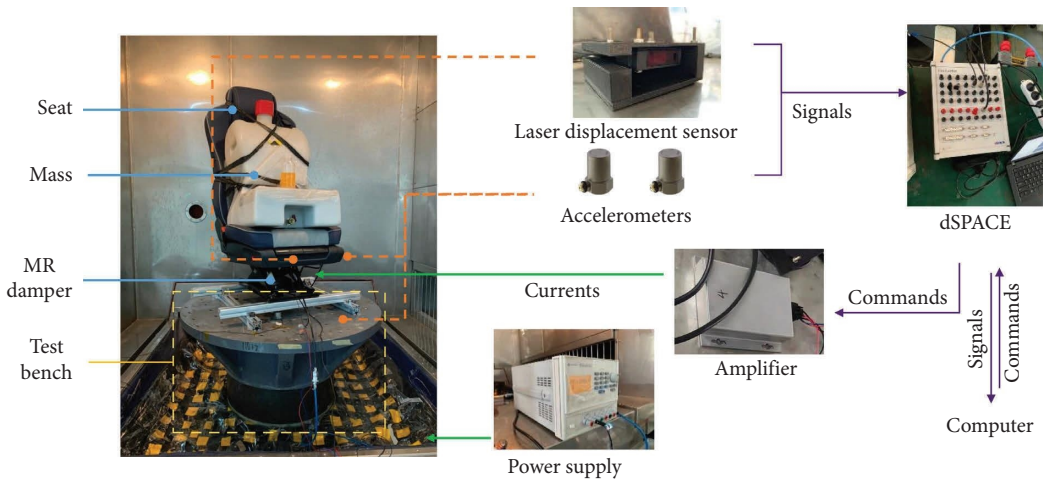

Figure 27: Experimental setup with controller and data acquisition system.

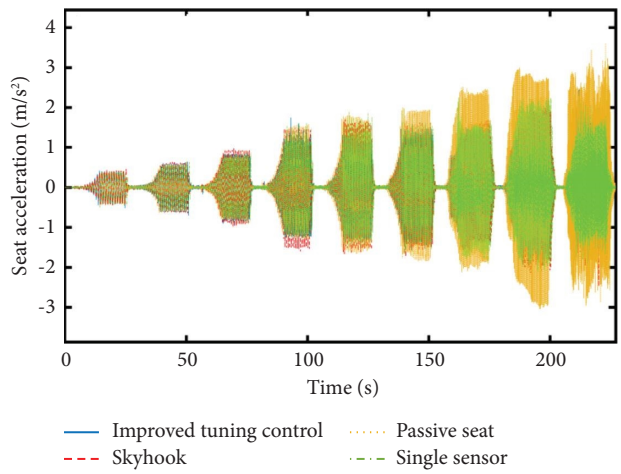

Figure 28: Seat acceleration response under different harmonic excitation frequencies.

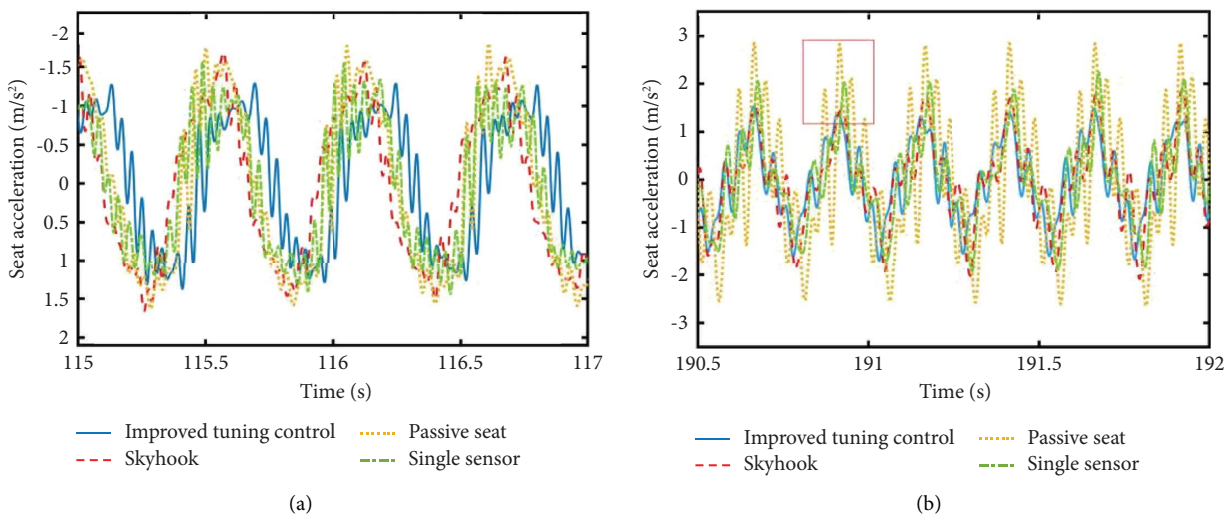

Figure 29: Continued.

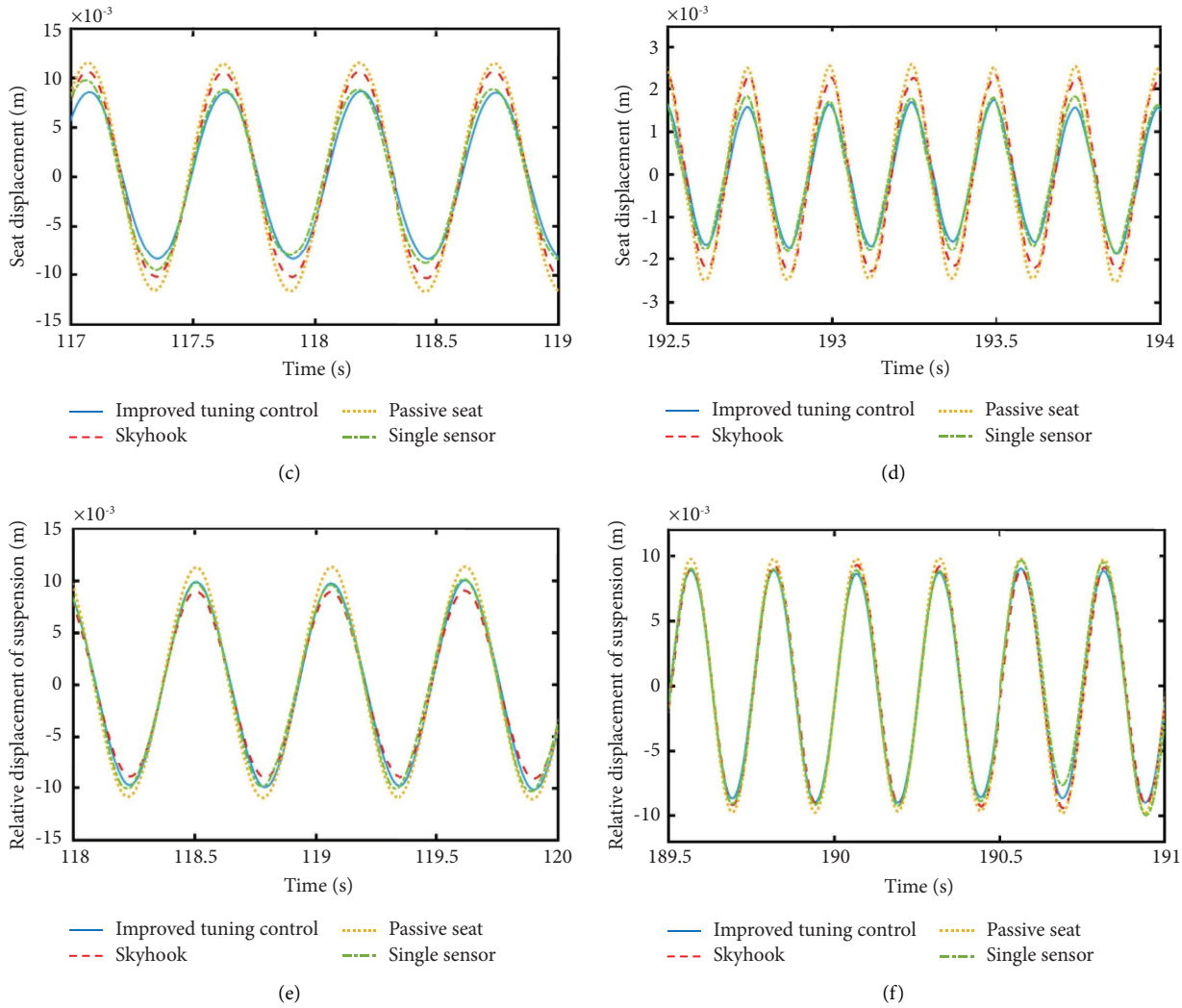

Figure 29: The dynamic responses under harmonic excitation in different frequencies. (a) Seat acceleration at 1.8 Hz. (b) Seat acceleration at 4 Hz. (c) Seat displacement at 1.8 Hz. (d) Seat displacement at 4 Hz. (e) Suspension stroke at 1.8 Hz. (f) Suspension stroke at 4 Hz.

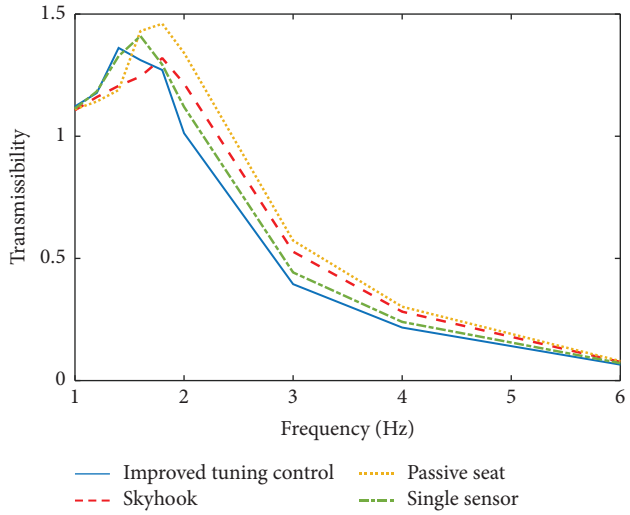

Figure 30: Transmissibility of seat suspension under harmonic excitation.

compared to the other three control cases. It is noted that the MS and single-sensor control cases have relatively high transmissibility at around 1 Hz, and there are several reasons. First, the accuracy of the frequency selector is affected by the jerk signal during vibration. Then, the seat suspension cannot move smoothly because of the friction and the damping force in some groups of the test, which causes the transmissibility to become lower than that of other results.

Figure 31 shows the control commands sent by dSPACE to control the current applied to the MR damper. When the seat vibrates at 1.8 Hz, Skyhook control keeps the longest time when current applies to the MR damper as the red curve shows. While the single-sensor control spends more time on the current application than the improved tuning control, it has too many jerks to maintain the current. As a result, the Skyhook control shows better performance than improved tuning control and single-sensor control at this frequency. It means that high and long-lasting

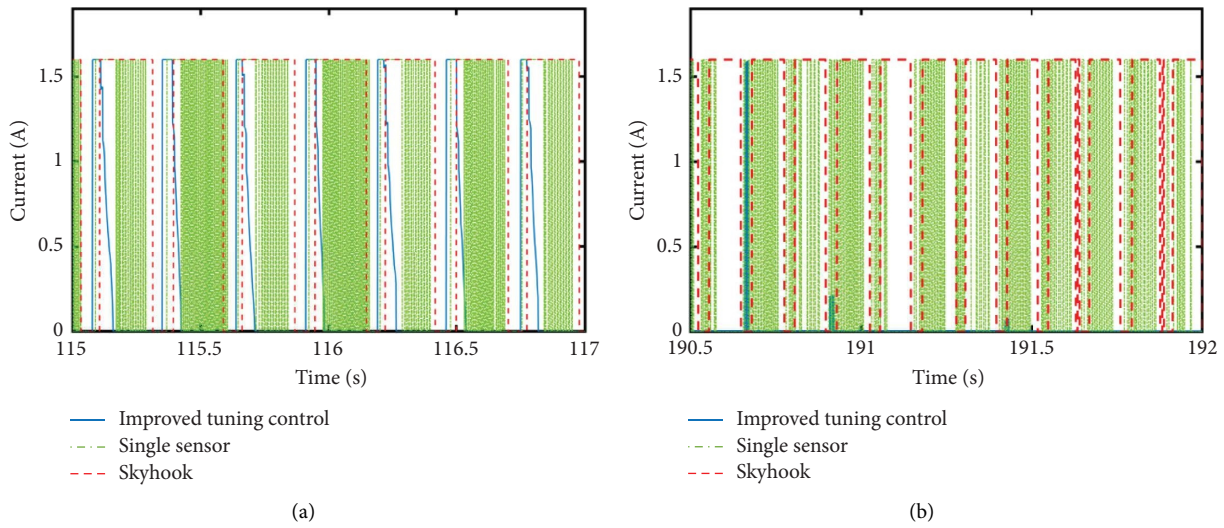

Figure 31: Current command signals in different frequencies. (a) Current commands at 1.8 Hz. (b) Current commands at 4 Hz.

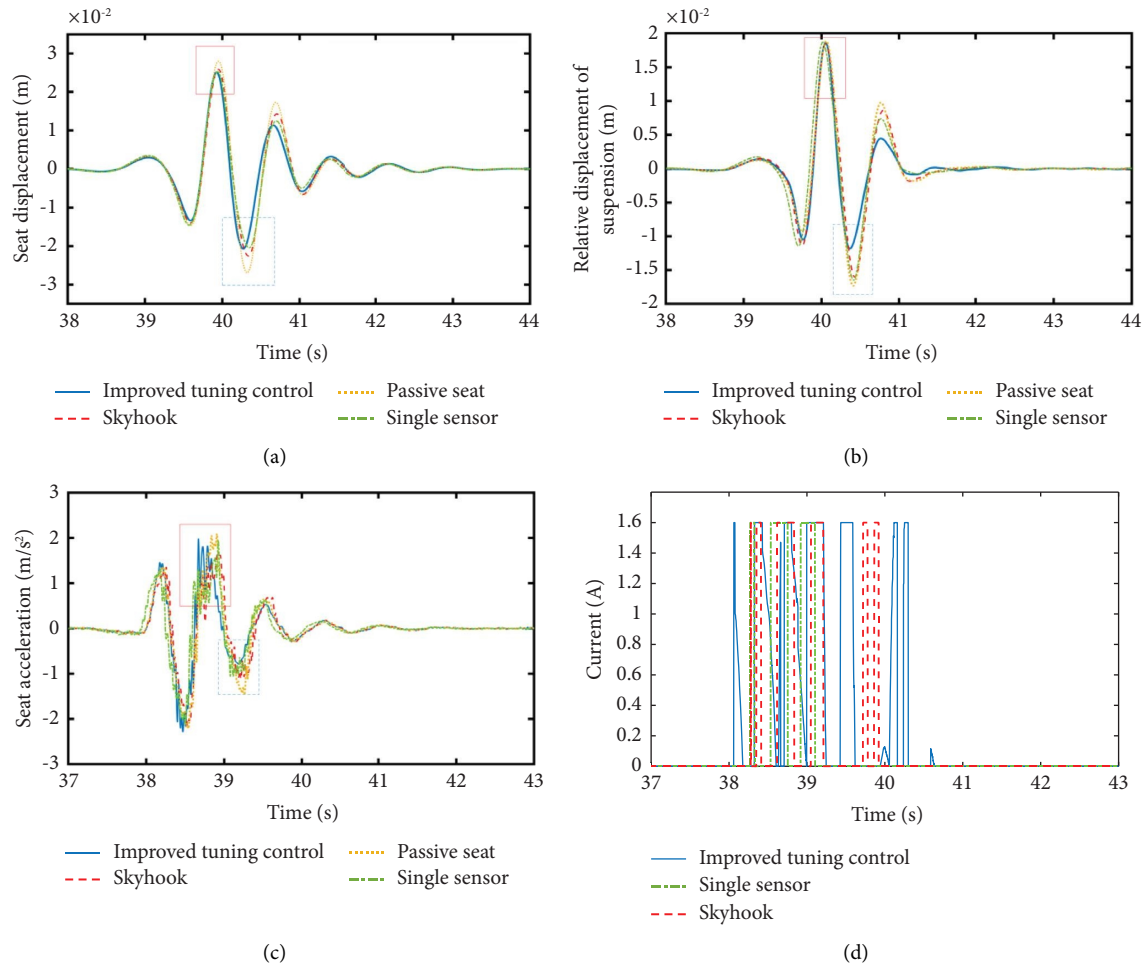

Figure 32: Bump excitation test results. (a) Seat displacement. (b) Relative displacement of seat suspension. (c) Seat acceleration. (d) Current command signals.

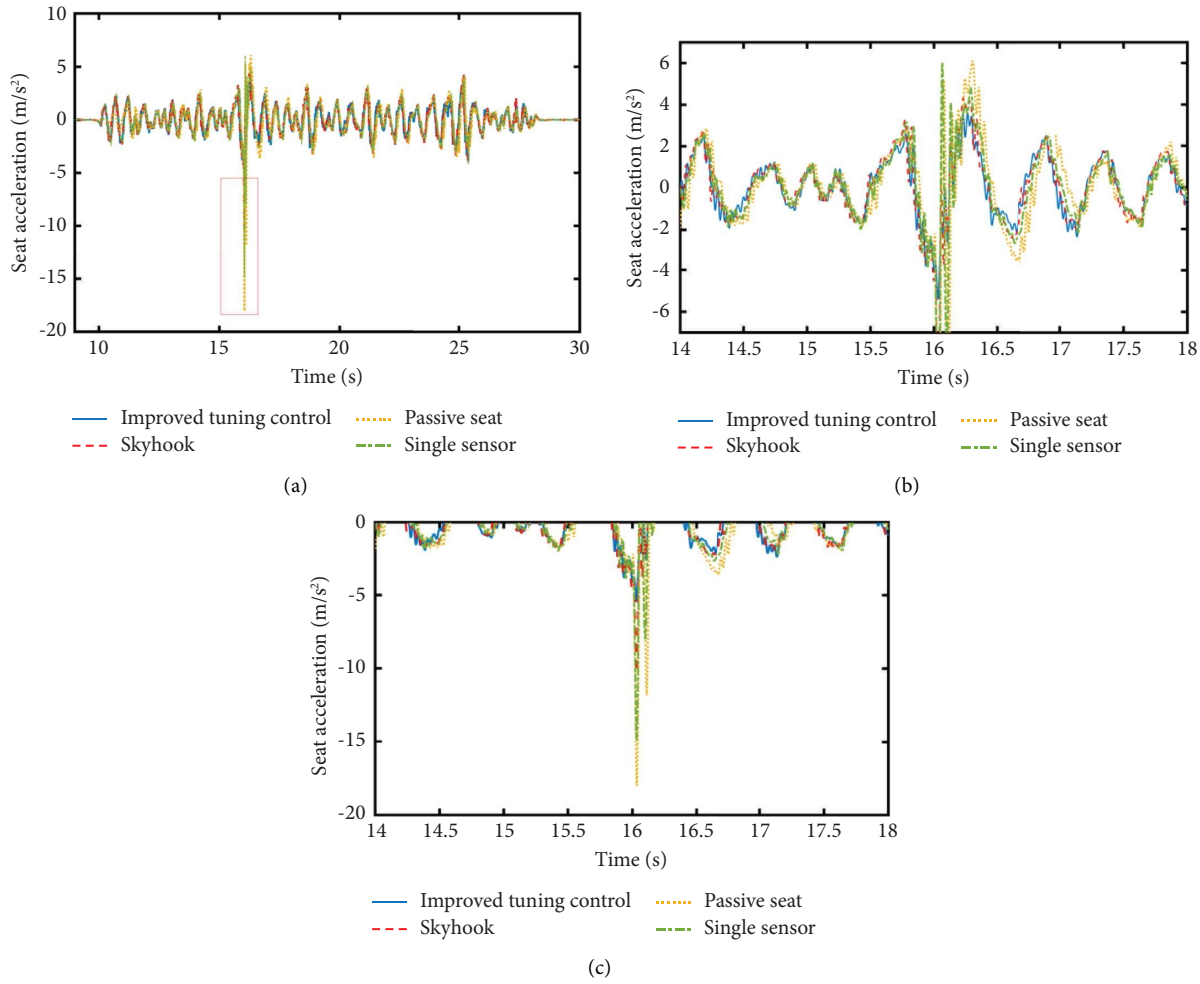

Figure 33: Seat acceleration results of random road excitation test. (a) General view of seat acceleration. (b) Detailed view of seat acceleration. (c) Detailed view of obvious jerking in seat acceleration.

damping can reduce the vibration at a relatively low frequency, which fits the analysis in Section 3.2. Additionally, improved tuning control gets good performance with short current supply without jerks, which means it is efficient. When the seat vibrates at 4 Hz, it needs small damping to reduce the seat acceleration and improve comfort as Section 3.2 discusses. Obviously, improved tuning control gives the best performance in Figure 31(b). Only slight current is applied to the MR damper while two other strategies are still supplying current. Hence, improved tuning control gets the best results in the relatively high-frequency range as Figure 30 shows, and the analysis in Section 3.2 can be proved.

4.2.2. Bump Excitation Test. The detailed results are shown in Figure 32. The improved tuning control case has a smaller seat displacement than the other cases, as shown in Figure 32(a), which is a 25% peak-peak reduction. Additionally, a smaller seat suspension stroke range for the improved tuning control case can be observed in the blue dotted box in Figure 32(b), which can reach the largest peak-peak suspension stroke reduction of 35%. This is much better than the other three cases, which verifies that the strategy has the best performance in avoiding end-stop impacts. Although the improved tuning control shows larger jerks in the acceleration signals than the other cases, as presented in the red solid box in Figure 32(c), the jerks, in this case, are reduced quickly, as presented in the blue dotted box in Figure 32(c). This indicates that the suspension with the improved tuning control strategy can respond quickly when it experiences a shock or impact. It is as shown in noted that improved tuning control provides the longest and most stable current in Figure 32(d). The current is kept after the largest shock at 40 s so that the relative displacement of the seat is reduced more quickly than others.

4.2.3. Random Road Excitation Test. The seat acceleration results are shown in Figure 33. It can be seen that the improved tuning control produces the lowest seat acceleration and seat jerking in the time domain, as shown in Figure 33(b). Therefore, the improved tuning control case shows the best acceleration attenuation performance with the largest shock, as shown in Figure 33(c), which

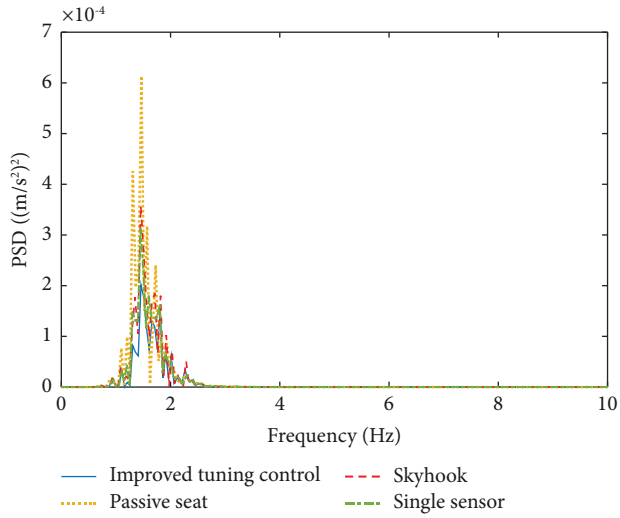

Figure 34: Power spectral density of seat suspension.

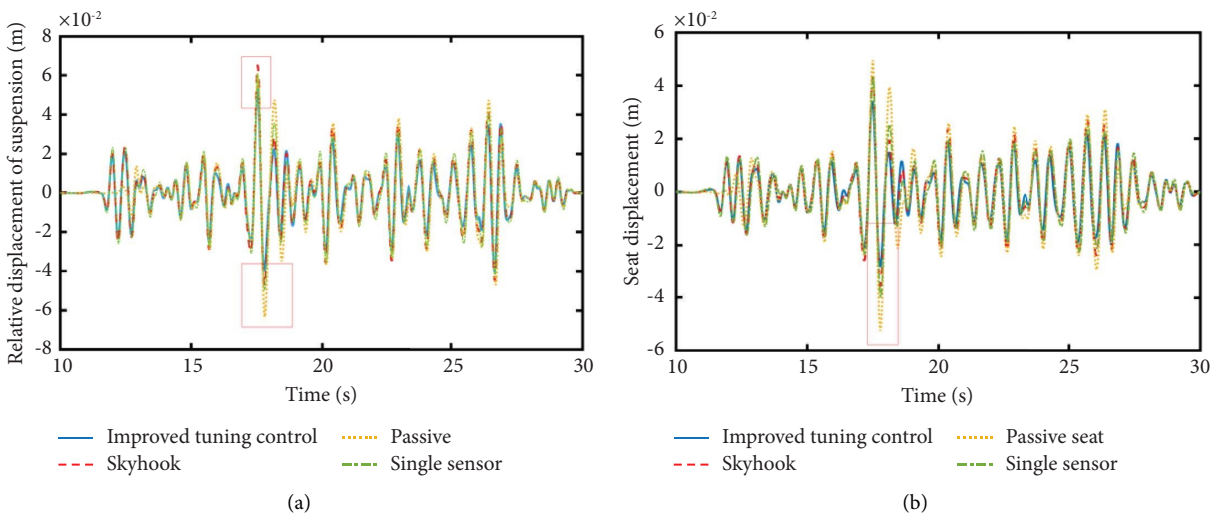

Figure 35: Random road excitation test results. (a) Relative displacement of seat suspension. (b) Seat displacement.

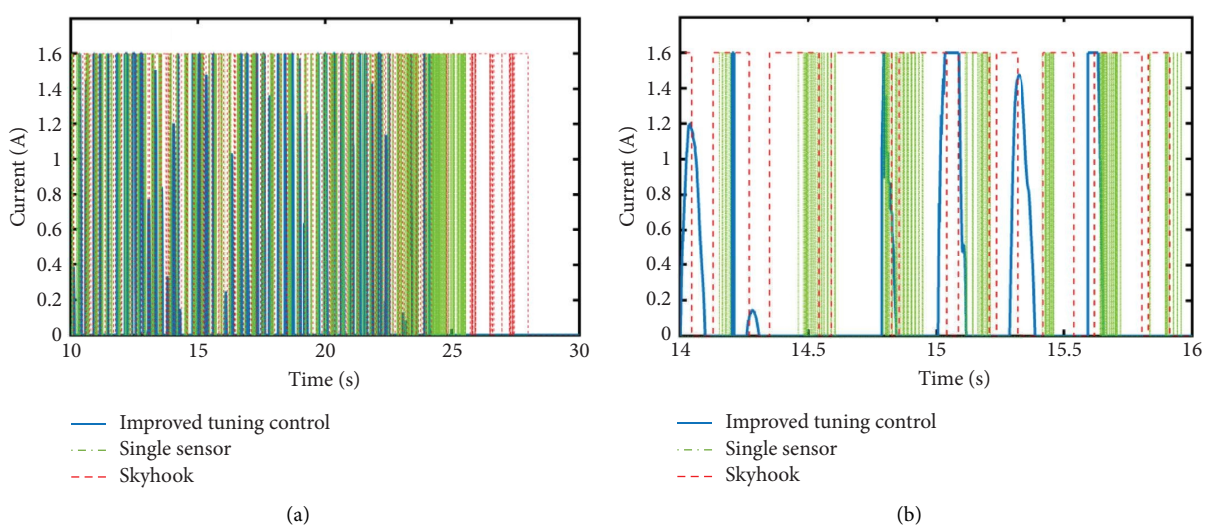

Figure 36: Current command signals of different control strategies. (a) Current command signals. (b) Detailed current signals.

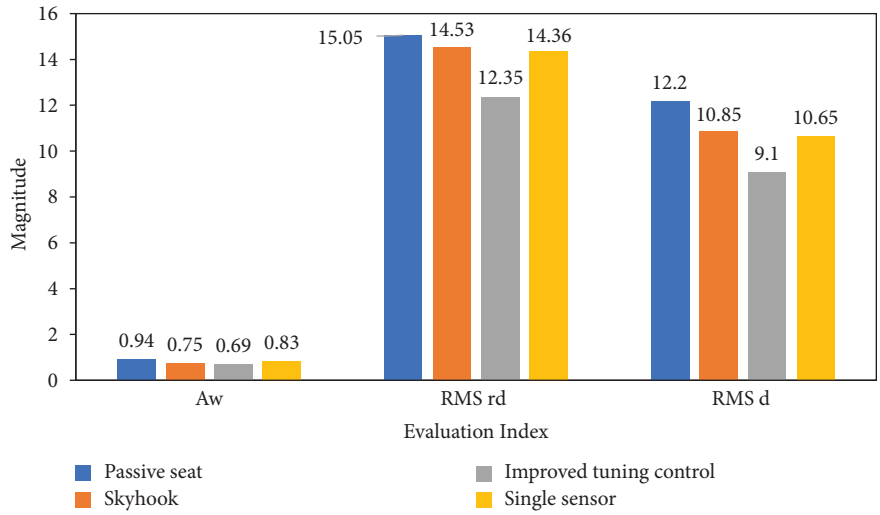

Figure 37: Results comparison of three indices.

demonstrates that the seat suspension with improved tuning control can reduce impacts when a serious shock is experienced. The results in the frequency domain, as shown in Figure 34, show the same conclusion, and the improved tuning control cases have a 30% reduction compared with the passive control seat case around the dominant frequency of the vibration at 1.8 Hz. The seat displacement and suspension stroke results are shown in Figure 35. It is noted that the improved tuning control case also has the best performance in terms of amplitude reduction, and the effects increase with the rise of the amplitudes. Notably, the suspension stroke of the passive seat case is larger than 60 mm, as shown in the red box in Figure 35(a), which means the suspension stroke is larger than the upper limit of seat suspension and end-stop impacts. The red box in Figure 35(a) is an obvious jerk in the acceleration signals indicating the end-stop impacts. The improved tuning control case has the best performance in solving this problem, which demonstrates that seat suspension with improved tuning control can greatly avoid end-stop impacts.

In Figure 36, the results are similar to Section 4.2.1. Skyhook control maintains a long-lasting current while single-sensor control cannot hold it, which causes different performances of them. Although providing relative short-time current to MR damper, the proposed tuning control strategy gives adequate damping force to avoid the end-stop impact as shown in Figure 34. Hence, it has good performance during the test.

The vibration control performances of the seat suspension with different control strategies are compared in Figure 37 in terms of the Aw, RMS rd, and RMS d as identified in Section 3.4.3. The improved tuning control case has the smallest values on all the indices, with Aw, RMS rd, and RMS d magnitude reductions of 26.6%, 17.9%, and 25.4% compared to the passive control seat case. This verifies that the improved tuning control can provide the best performance. As a result, the MR seat suspension with the proposed control strategy can largely reduce the vibration level and greatly avoid end-stop impact.

5. Conclusions

A seat suspension system was installed with MR dampers controlled by the improved tuning control strategy to improve seat comfort and avoid end-stop impacts in this study. An MR damper was designed and verified the characteristics via damper performance testing, and the damping force with the same current is slightly different up to 10% during the varying excitation frequency. A mathematical model of seat prototype suspension was established with the measurement data, and the model could greatly predict the experimental results with differences lower than 9%. An improved tuning control strategy based on a frequency selector was proposed to adjust the damping force of the MR damper, which includes the no-jerk improvement and end-stop impact countermeasures. Numerical simulations and experiments for the harmonic, bump, and random road excitations were conducted to evaluate the vibration control performance of the seat suspension. Both the simulations and experiments prove that the MR seat suspension with the proposed algorithm can largely improve seat comfort and greatly avoid end-stop impact, which has an approximately 20% improvement compared with the passive control seat suspension.

Data Availability

The data used to support the findings of the study are available from the corresponding author upon request.

Conflicts of Interest

The authors declare that they have no conflicts of interest.

Acknowledgments

The authors would like to acknowledge the support provided by the National Science Foundation of China (Grant ref. 52075056) and the Graduate Scientific Research and

Innovation Foundation of Chongqing, China (Grant ref. CYB19009). The authors would also like to appreciate the funding support by the Innovation and Technology Commission (ITC) of Hong Kong SAR Government to the Hong Kong Branch of Chinese National Rail Transit Electrification and Automation Engineering Technology Research Center (Grant ref. K-BBY1) and the Hong Kong Polytechnic University to start-up fund for RAPs under the Strategic Hiring Scheme (Grant ref. 1-BD22).

References

[1] R. P. Blood, M. G. Yost, J. E. Camp, and R. P. Ching, "Whole-body vibration exposure intervention among professional bus and truck drivers: a laboratory evaluation of seat-suspension designs," *Journal of Occupational and Environmental Hygiene*, vol. 12, no. 6, pp. 351–362, 2015.

[2] A. Burdorf and P. Swuste, "The effect of seat suspension on exposure to whole-body vibration of professional drivers," *Annals of Occupational Hygiene*, vol. 37, no. 1, pp. 45–55, 1993.

[3] L. Deng, S. S. Sun, M. Christie et al., "Investigation of a seat suspension installed with compact variable stiffness and damping rotary magnetorheological dampers," *Mechanical Systems and Signal Processing*, vol. 171, Article ID 108802, 2022.

[4] I. Maciejewski, L. Meyer, and T. Krzyzynski, "Modelling and multi-criteria optimisation of passive seat suspension vibro-isolating properties," *Journal of Sound and Vibration*, vol. 324, no. 3-5, pp. 520–538, 2009.

[5] A. Agharkakli, G. S. Sabet, and A. Barouz, "Simulation and analysis of passive and active suspension system using quarter car model for different road profile," *International Journal of Engineering Trends and Technology*, vol. 3, pp. 636–644, 2012.

[6] L. L. Zhao, Y. W. Yu, C. C. Zhou, and F. X. Yang, "Modelling and validation of a seat suspension with rubber spring for off-road vehicles," *Journal of Vibration and Control*, vol. 24, no. 18, pp. 4110–4121, 2018.

[7] M. Yu, C. R. Liao, W. M. Chen, and S. L. Huang, "Study on MR semi-active suspension system and its road testing," *Journal of Intelligent Material Systems and Structures*, vol. 17, no. 8-9, pp. 801–806, 2006.

[8] S. S. Sun, J. Yang, P. H. Wang et al., "Experimental study of a variable stiffness seat suspension installed with a compact rotary MR damper," *Frontiers in Materials*, vol. 8, Article ID 594843, 2021.

[9] D. S. Yoon, G. W. Kim, and S. B. Choi, "Response time of magnetorheological dampers to current inputs in a semi-active suspension system: modeling, control and sensitivity analysis," *Mechanical Systems and Signal Processing*, vol. 146, Article ID 106999, 2021.

[10] D. H. Ning, S. S. Sun, L. D. Wei, B. J. Zhang, H. P. Du, and W. H. Li, "Vibration reduction of seat suspension using observer based terminal sliding mode control with acceleration data fusion," *Mechatronics*, vol. 44, pp. 71–83, 2017.

[11] W. X. Li, H. P. Du, D. H. Ning, W. H. Li, S. S. Sun, and J. Wei, "Event-triggered H∞ control for active seat suspension systems based on relaxed conditions for stability," *Mechanical Systems and Signal Processing*, vol. 149, Article ID 107210, 2021.

[12] F. Viadero-Monasterio, B. L. Boada, M. Boada, and V. Díaz, "H-infinity dynamic output feedback control for a networked control active suspension system under actuator faults," *Mechanical Systems and Signal Processing*, vol. 162, Article ID 108050, 2022.

[13] D. C. Karnopp, M. J. Crosby, and R. A. Harwood, "Vibration control using semi-active force generators," *Journal of Engineering for Industry*, vol. 96, no. 2, pp. 619–626, 1974.

[14] A. Heidarian and X. Wang, "Review on seat suspension system technology development," *Applied Sciences*, vol. 9, no. 14, p. 2834, 2019.

[15] X. C. Zhu, X. J. Jing, and L. Cheng, "Magnetorheological fluid dampers: a review on structure design and analysis," *Journal of Intelligent Material Systems and Structures*, vol. 23, no. 8, pp. 839–873, 2012.

[16] Y. J. Zhang, J. X. Guo, J. W. Yang, and X. Li, "Recent structural developments and applications of magnetorheological dampers (mrd): a review," *Magnetochemistry*, vol. 9, no. 4, p. 90, 2023.

[17] W. Hu and N. M. Wereley, "Magnetorheological fluid and elastomeric lag damper for helicopter stability augmentation," *International Journal of Modern Physics B*, vol. 19, no. 7, pp. 1471–1477, 2005.

[18] S.-B. Choi, M.-H. Nam, and B.-K. Lee, "Vibration control of a MR seat damper for commercial vehicles," *Journal of Intelligent Material Systems and Structures*, vol. 11, no. 12, pp. 936–944, 2000.

[19] S.-B. Choi and Y.-M. Han, "MR seat suspension for vibration control of a commercial vehicle," *International Journal of Vehicle Design*, vol. 31, no. 2, pp. 202–215, 2003.

[20] G. J. Stein, "Results of investigation of an electropneumatic active vibration control system for a driver's seat," *Proceedings of the Institution of Mechanical Engineers-Part D: Journal of Automobile Engineering*, vol. 209, no. 3, pp. 227–234, 1995.

[21] S. S. Sun, D. H. Ning, J. Yang, H. Du, S. W. Zhang, and W. H. Li, "A seat suspension with a rotary magnetorheological damper for heavy duty vehicles," *Smart Materials and Structures*, vol. 25, no. 10, Article ID 105032, 2016.

[22] S. M. Savaresi, E. Silani, and S. Bittanti, "Acceleration-driven-damper (ADD): an optimal control algorithm for comfort-oriented semiactive suspensions," *Journal of Dynamic Systems, Measurement, and Control*, vol. 127, no. 2, pp. 218–229, 2005.

[23] S. M. Savaresi and C. Spelta, "Mixed sky-hook and ADD: approaching the filtering limits of a semi-active suspension," *Journal of Dynamic Systems, Measurement, and Control*, vol. 129, no. 4, pp. 382–392, 2007.

[24] D. Sammier, O. Sename, and L. Dugard, "Skyhook and H8 control of semi-active suspensions: some practical aspects," *Vehicle System Dynamics*, vol. 39, no. 4, pp. 279–308, 2003.

[25] R. Morselli and R. Zanasi, "Control of port Hamiltonian systems by dissipative devices and its application to improve the semi-active suspension behaviour," *Mechatronics*, vol. 18, no. 7, pp. 364–369, 2008.

[26] S. Rakheja and S. Sankar, "Vibration and shock isolation performance of a semi-active on-off damper," *Journal of Vibration and Acoustics*, vol. 107, no. 4, pp. 398–403, 1985.

[27] R. S. Sharp and H. Peng, "Vehicle dynamics applications of optimal control theory," *Vehicle System Dynamics*, vol. 49, no. 7, pp. 1073–1111, 2011.

[28] X.-M. Du, M. Yu, J. Fu, Y.-X. Peng, H.-F. Shi, and H. Zhang, "H control for a semi-active scissors linkage seat suspension with magnetorheological damper," *Journal of Intelligent Material Systems and Structures*, vol. 30, no. 5, pp. 708–721, 2019.

[29] D. K. Shin, D. X. Phu, S.-M. Choi, and S.-B. Choi, "An adaptive fuzzy sliding mode control of magneto-rheological seat suspension with human body model," *Journal of*

Intelligent Material Systems and Structures, vol. 27, no. 7, pp. 925–934, 2016.

[30] D. X. Phu, J.-H. An, and S.-B. Choi, "A Novel adaptive PID Controller with application to vibration control of a semi-active vehicle seat suspension," *Applied Sciences*, vol. 7, no. 10, p. 1055, 2017.

[31] X. Liu, N. Wang, K. Wang et al., "Optimizing vibration attenuation performance of a magnetorheological damper-based semi-active seat suspension using artificial intelligence," *Frontiers in Materials*, vol. 6, p. 269, 2019.

[32] S. D. Nguyen, Q. H. Nguyen, and S.-B. Choi, "A hybrid clustering based fuzzy structure for vibration control – Part 2: an application to semi-active vehicle seat-suspension system," *Mechanical Systems and Signal Processing*, vol. 56-57, pp. 288–301, 2015.

[33] T. Hashiyama, T. Furuhashi, and Y. Uchikawa, "A study on finding fuzzy rules for semi-active suspension controllers with genetic algorithm," in *Proceedings of 1995 IEEE International Conference on Evolutionary Computation*, pp. 279–289, Perth, Australia, December 1995.

[34] M. Ahmadian, B. Reichert, X. Song, and S. S. Southward, "No-jerk semi-active skyhook control method and apparatus," Virginia Tech Intellectual Properties Inc, Blacksburg, VA, USA, US6115658 A, 2000.

[35] N. M. Kwok, Q. P. Ha, J. Li, T. H. Nguyen, B. Samali, and B. Samali, "A novel hysteretic model for magnetorheological fluid dampers and parameter identification using particle swarm optimization," *Sensors and Actuators A: Physical*, vol. 132, no. 2, pp. 441–451, 2006.

[36] S. M. Savaresi and C. Spelta, "A single-sensor control strategy for semi-active suspensions," *IEEE Transactions on Control Systems Technology*, vol. 17, no. 1, pp. 143–152, 2009.

[37] International Organization for Standardization, *ISO 2631-1: Mechanical Vibration and Shock-Evaluation of Human Exposure to Whole-Body Vibration-Part1: General Requirements*, International Organization for Standardization, Genva, Switzerland, 1997.